Clim. Past, 15, 2031–2051, 2019
https://doi.org/10.5194/cp-15-2031-2019

Climate of the Past
Open Access
EGU

A 120 000-year record of sea ice in the North Atlantic?

Niccolò Maffezzoli[1,2], Paul Vallelonga[2], Ross Edwards[3,4], Alfonso Saiz-Lopez[5], Clara Turetta[1,6], Helle Astrid Kjær[2], Carlo Barbante[1,6], Bo Vinther[2], and Andrea Spolaor[1,6]

[1]Institute of Polar Sciences, ISP-CNR, Via Torino 155, 30172 Venice, Italy
[2]Physics of Ice, Climate and Earth (PICE), Niels Bohr Institute, University of Copenhagen, Tagensvej 16, 2200 Copenhagen, Denmark
[3]Physics and Astronomy, Curtin University of Technology, Kent St, Bentley, WA 6102, Perth, Australia
[4]Department of Civil and Environmental Engineering, UW-Madison, Madison, WI 53706, USA
[5]Department of Atmospheric Chemistry and Climate, Institute of Physical Chemistry Rocasolano, CSIC, Madrid, Spain
[6]Department of Environmental Sciences, Informatics and Statistics, Ca' Foscari University of Venice, Via Torino 155, 30170 Venice, Italy

Correspondence: Niccolò Maffezzoli (niccolo.maffezzoli@unive.it)

Received: 2 July 2018 – Discussion started: 17 July 2018
Revised: 2 November 2019 – Accepted: 15 November 2019 – Published: 19 December 2019

Abstract. Although it has been demonstrated that the speed and magnitude of the recent Arctic sea ice decline is unprecedented for the past 1450 years, few records are available to provide a paleoclimate context for Arctic sea ice extent. Bromine enrichment in ice cores has been suggested to indicate the extent of newly formed sea ice areas. Despite the similarities among sea ice indicators and ice core bromine enrichment records, uncertainties still exist regarding the quantitative linkages between bromine reactive chemistry and the first-year sea ice surfaces. Here we present a 120 000-year record of bromine enrichment from the RECAP (REnland ice CAP) ice core, coastal east Greenland, and interpret it as a record of first-year sea ice. We compare it to existing sea ice records from marine cores and tentatively reconstruct past sea ice conditions in the North Atlantic as far north as the Fram Strait (50–85° N). Our interpretation implies that during the last deglaciation, the transition from multi-year to first-year sea ice started at ∼ 17.5 ka, synchronously with sea ice reductions observed in the eastern Nordic Seas and with the increase in North Atlantic ocean temperature. First-year sea ice reached its maximum at 12.4–11.8 ka during the Younger Dryas, after which open-water conditions started to dominate, consistent with sea ice records from the eastern Nordic Seas and the North Icelandic shelf. Our results show that over the last 120 000 years, multi-year sea ice extent was greatest during Marine Isotope Stage (MIS) 2 and possibly during MIS 4, with more extended first-year sea ice during MIS 3 and MIS 5. Sea ice extent during the Holocene (MIS 1) has been less than at any time in the last 120 000 years.

1 Introduction: Br_{enr} as a potential indicator of past sea ice conditions

The connection between Arctic sea ice and bromine was first identified through an anticorrelation between springtime ground level ozone (O_3) and filterable bromine air concentrations (Barrie et al., 1988). Large bromine oxide (BrO) column enhancements and simultaneous tropospheric ozone depletion were later found in Antarctica (Kreher et al., 1997). Satellite observations reveal geographically widespread "bromine explosions", i.e. the sudden increase in atmospheric bromine concentrations during springtime occurring in both polar regions (Chance, 1998; Richter et al., 1998; Wagner and Platt, 1998). The mechanism proceeds via springtime photochemical heterogeneous reactions that lead to the activation of bromide, followed by the release and exponential increase in gas-phase bromine species in the polar troposphere (Vogt et al., 1996). Several saline substrates on fresh sea ice surfaces (hereafter referred to as first-year sea ice, FYSI) were suggested as reservoirs of reactive sea-salt aerosols (SSAs) capable of sustaining bromine recycling (Abbatt et al., 2012; Saiz-Lopez and von Glasow, 2012). To

date, both model studies (Yang et al., 2008, 2010) and experimental evidence (Pratt et al., 2013; Zhao et al., 2016; Frey et al., 2019) consider the deposited snow layer on FYSI (known as salty blowing snow) to be the most efficient substrate for SSA release and bromine activation.

Atmospheric bromine and sodium thus originate from both oceanic and FYSI sea-salt aerosols, where their concentration ratio is that of seawater mass: $(Br/Na)_m = 0.0062$ (the subscript indicates "marine", Millero et al., 2008). Br_{enr} values in ice core records, i.e. the bromine-to-sodium mass ratios beyond the seawater value (Eq. 1), were introduced by Spolaor et al. (2013b) as a potential proxy for past FYSI conditions within the ocean region influencing the ice core location. The basic assumption behind this idea is that bromine recycling on FYSI surfaces would increase the bromine-to-sodium mass ratio beyond the seawater value in the atmosphere and at the ice core location, thus isolating the effect of FYSI-induced bromine recycling from the sea-salt aerosol contribution, the latter being interfered with by oceanic emissions. Further studies have provided some evidence on the validity of Br_{enr} as an FYSI indicator (Spolaor et al., 2013a, 2014, 2016a). At present, however, this interpretation is still challenged by several uncertainties related to the different variables which play a role in the chemical and physical processes involved (Abbatt, 2013). These can be grouped into three categorizes: bromine activation, transport, and deposition or postdeposition. They are briefly discussed here and in Appendix A.

Pratt et al. (2013) showed that saline snow collected on Arctic tundra or first-year sea ice surfaces can serve as an efficient reservoir for bromine activation. They point out, however, that the acidity of snow is a prerequisite for bromine activation, as well as internal snowpack air chemistry (e.g. the concentration of $^{\cdot}OH$, NO_3^-/NO_2^-). A modification in these factors would alter the bromine production efficiency at constant FYSI extent. Aged sea ice (second-year sea ice or older) possibly contributes to bromine activation due to a non-zero salt content, but the amount of this second-order source effect is unknown.

Bromine travels from the source region to the ice core location both in the aerosol and gas phases, while sodium is only found in the aerosol phase. To date, the partitioning of bromine species between the two phases is not clear. Additionally, some studies have reported that bromine recycling takes place within the plume even during the transport (Zhao et al., 2016), leading to possible bromine depletion from the aerosol in favour to the gas phase. Overall, the final observed Br_{enr} values in ice samples depend on the relative importance of aerosol and gas-phase bromine partitioning. It appears that fine aerosols are enriched in bromine, while coarse particles are depleted (Legrand et al., 2016, Theodore Koenig, personal communication, 2018). Additionally, the two phases likely have a different atmospheric residence time; thus, the final bromine-to-sodium ratio found in the snow might be a function of the transport duration. In general, bromine-reactive surfaces would increase the atmospheric residence time of bromine species, enhancing the bromine-to-sodium ratios away from the sea ice or ocean sources. On this topic, from springtime Arctic snow samples collected from a transect directed inland, Simpson et al. (2005) showed that sodium is deposited faster than bromine, suggesting a role of longer-lasting gas-phase bromine (Fig. 3 in their study). From samples collected during a coast-to-inland Antarctic transect (Zhongshan Station–Dome A), Li et al. (2014) showed much reduced spatial gradients between sodium and bromine snow concentrations when compared to Simpson and co-workers (Fig. 2 in Li et al., 2014). In a similar inland-directed Antarctic transect (Talos Dome–Dome C), Spolaor et al. (2013b) presented simultaneous bromine and sodium deposition fluxes from three sites and a model run aimed at explaining the experimental results (Fig. 6 in their study). The authors note that for their results to be explained by the model, the deposition velocity of HBr needs to be set at least 3 times larger than the average sea-salt aerosol deposition velocity. To conclude, the interference of transport processes with the sea ice source effects in either the Arctic or Antarctica is not clear and should be further investigated.

The last set of uncertainties relates to the variables associated with the deposition of bromine and sodium, such as the variability in accumulation rates over long timescales, which would impact the relative importance of the wet and dry contributions of the two species. Finally, photolytic reemission of bromine from the snowpack could be responsible for bromine loss and decreased Br_{enr} values. A dedicated discussion of this last topic can be found in Appendix A.

We acknowledge the above-mentioned open questions on the validity of Br_{enr} as an FYSI proxy and clearly point out that further studies are needed to shed light on these uncertainties. We thus proceed with the interpretation of Br_{enr} as an FYSI proxy bearing in mind that other variables could, at present, explain a Br_{enr} record.

Here, we consider the available evidence regarding past sea ice conditions in the North Atlantic and present a bromine enrichment record from the RECAP (REnland ice CAP) ice core, located in coastal east Greenland. Because of its location, RECAP should record the fingerprint of sea ice in the North Atlantic. We compare our RECAP Br_{enr} record with sea ice reconstructions from five marine sediment cores drilled within the Renland source area: the Fram Strait, the Norwegian Sea and the North Icelandic shelf (Fig. 1).

2 Methods

2.1 The 2015 RECAP ice core

The RECAP ice core was retrieved from the Renland ice cap (71°18′18″ N, 26°43′24″ W; 2315 m a.s.l.) from 13 May to 12 June 2015. The ice cap is located on the Renland peninsula and is independent of the main Greenland ice sheet, with fjords to the north and south. A 98 mm diameter ice core

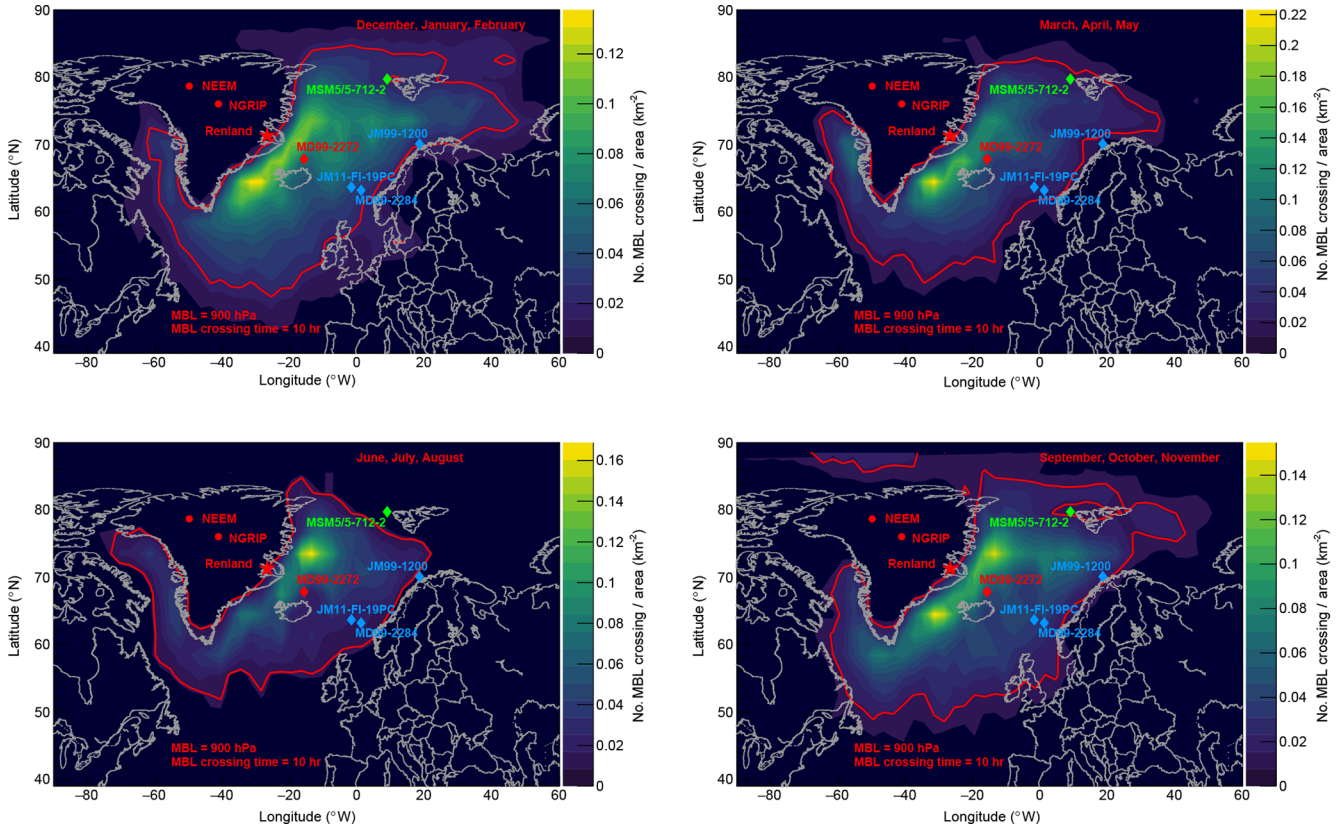

Figure 1. Modern (2000–2016) source region of atmospheric sodium and bromine deposited at the Renland site estimated from 3 d back trajectory calculations. On the z axis is represented the number of marine boundary layer (MBL) crossings per unit area, derived by selecting only those trajectories which crossed the 900 hPa isosurface for at least 10 h (see Sect. 2.3). The red line contours 75 % of the distribution integral, and it is considered to be the bromine and sodium source region. It covers the North Atlantic Ocean from ∼ 50 to 85° N. A minor contribution is expected from west Greenland waters. Note that areas outside the 75 % line with counts < 0.02 crossings km^{-2} are not coloured. The analysis is performed on a seasonal basis. The Renland ice cap is marked with a star; the NEEM and NGRIP core sites are marked with a circle. The diamonds indicate the marine cores discussed in the text: Svalbard margin (MSM5/5-712-2, Müller and Stein, 2014), North Icelandic shelf (MD99-2272, Xiao et al., 2017) and the Norwegian Sea (JM11-FI-19PC, Hoff et al., 2016; MD99-2272, Muschitiello et al., 2019; JM99-1200, Cabedo-Sanz et al., 2013).

was recovered to 584 m (bedrock). The drilling occurred in a dry borehole to 130 m depth, and estisol 140 drilling fluid was used for the remaining depth. The record covers the last 120 800 years. The core age model is described in full details in the Supplement of Simonsen et al. (2019).

The ice core samples dedicated to mass spectroscopy measurements ($n = 1205$) were collected and automatically decontaminated by a continuous ice core melting system as part of the RECAP Continuous Flow Analysis (CFA) campaign conducted at the University of Copenhagen in Autumn 2015. The ice core was melted at a speed of approx. 3 cm min^{-1} on a gold-coated plate copper melter head (Bigler et al., 2011; Kaufmann et al., 2008). Meltwater was collected continuously from the melter head into polyethylene vials precleaned with ultrapure water (> 18.2 MΩ cm^{-1}) at two different depth resolutions. From the ice cap surface to a depth of 535.15 m, samples incorporated ice meltwater spanning depths of 55 cm. From a depth of 535.15 m to the ice cap bedrock, the samples integrated 18.3 cm. The time resolution is annual to multicentennial in the Holocene and centennial to millennial in the glacial section. After collection, the samples were immediately refrozen at −30 °C and kept in the dark until mass spectroscopy analyses to reduce bromine photolysis reactions.

2.2 Ice core measurements: determination of Br, Na, Cl, Ca and Mg

The samples were shipped to Ca' Foscari University of Venice (Italy, $n = 770$) and Curtin University of Technology (Perth, Australia, $n = 435$) for determination of bromine (Br), sodium (Na), chlorine (Cl), calcium (Ca) and magnesium (Mg) by inductively coupled plasma mass spectroscopy (ICP-MS). Only bromine and sodium were measured in the samples analysed at the Italian lab, while all elements were quantified with the Australian set-up.

The depth and age ranges associated with the Italian samples are surface–150 m (2015 CE–328 years b2k), 165–219 m (383–636 years BP), 234–413 m (727–2857 years b2k) and 441–495 m (3522–5749 years b2k). The depth and age ranges associated with the Australian samples are 150–165 m (328–383 years b2k), 219–234 m (636–727 years b2k), 413–441 m (2857–3522 years b2k) and 495–562 m (5749–120 788 years b2k).

University Ca' Foscari of Venice, Italy. Bromine and sodium (^{79}Br and ^{23}Na) were determined by collision reaction cell inductively coupled plasma mass spectroscopy (CRC-ICP-MS, Agilent 7500cx, Agilent, California, USA). The introduction system consisted of an ASX-520 autosampler (CETAC Technologies, Omaha, USA) and Scott spray chamber fitted with a MicroFlow PFA (perfluoroalkoxy) nebulizer. The sample flow was kept at 100 µL min^{-1}. All reagents and standard solutions were prepared with ultrapure water (UPW; 18.2 M Ω cm^{-1}). Nitric acid (65 % v/v, trace metal grade, Romil, Cambridge, UK) and UPW washes (2 min each) were used for background recovery after every sample analysis. The nitric acid washing concentration was lowered to 2 %. The experimental routine (standards and calibrations) as well as the overall instrument performance (detection limits and reproducibility) are the same as in Spolaor et al. (2016b).

Curtin University of Technology, Perth, Australia. The analyses were performed by inductively coupled plasma sector field mass spectroscopy in reverse Nier–Johnson geometry (ICP-SFMS, Element XR, Thermo Fisher, Germany) inside a Class 100 clean room environment at the Curtin University TRACE facility (Trace Research Advanced Clean Environment Facility). The ICP-SFMS introduction system consisted of an Elemental Scientific Inc. (ESI, Omaha, USA) syringe-pumped autosampler (Seafast II) with a 1 mL PFA capillary injection loop and using an ultrapure water carrier. A 1 ppb indium internal standard in 5 % v/v nitric acid (HNO_3, double-PFA distilled) was mixed inline at a flow rate of 25 µL min^{-1} using a T-split (final flow rate of 400 µL min^{-1}, take-up time 1.5 min). Nebulization occurred in a peltier cooled (2 °C) quartz cyclonic spray chamber (PC3, ESI), fitted with a PFA micro-concentric nebulizer (PFA-ST, ESI). Bromine, sodium, magnesium, chlorine and calcium isotopes (^{79}Br, ^{23}Na, ^{24}Mg, ^{35}Cl, ^{44}Ca) were detected in medium resolution (10 % valley resolution of 4000 amu) and normalized to ^{115}In. Memory effects were reduced by rinsing the system between samples with high-purity HNO_3 (3 %) and UPW. One procedural blank and one quality-controlled standard (QC) were analysed every five samples to monitor the system stability. The detection limits, calculated as 3σ of the blank values ($n = 80$) were 0.18 ppb (Br), 1.1 ppb (Na), 0.2 ppb (Mg), 1.6 ppb (Ca) and 4.6 ppb (Cl). The majority of the sample concentrations were above the detection limits for all elements (> 97 %). The relative standard deviations of the control standard sample ($n = 82$) concentrations were monitored over > 100 h and were 9 % (Br), 4 % (Na), 3 % (Mg), 4 % (Ca) and 13 % (Cl). Calibration standards were prepared by sequential dilution (seven standards) of NIST traceable commercial standards (High-Purity Standards, Charleston, USA). All materials used for the analytical preparations were systematically cleaned with UPW (18.2 >M Ω cm^{-1}) and double-PFA distilled ultrapure HNO_3 (3 %, prepared from IQ grade HNO_3, Choice Analytical Pty Ltd, Australia) throughout.

A laboratory intercomparison between sodium and bromine measurements was performed on a common set of samples ($n = 140$) to investigate differences between the analytical techniques and laboratories, as described in Vallelonga et al. (2017). The correlations and the gradients between the measured concentrations in the two set-ups are $\rho(\mathrm{Na_{IT}\text{-}Na_{AUS}}) = 0.99$ ($n = 140$; $p < 0.01$), $m_{\mathrm{Na}} = 1.08 \pm 0.01$ (1σ) for sodium and $\rho(\mathrm{Br_{IT}\text{-}Br_{AUS}}) = 0.93$ ($n = 140$; $p < 0.01$), $m_{\mathrm{Br}} = 1.08 \pm 0.02$ (1σ) for bromine.

2.3 Atmospheric reanalysis: the source region of bromine and sodium for the RECAP ice core

To estimate the source of bromine and sodium deposited at Renland, daily back trajectories were calculated from 2000 CE to 2016 CE with HYSPLIT4 (Stein et al., 2015; Draxler et al., 1999; Draxler and Hess, 1998, 1997), using publicly available NCEP/NCAR Global Reanalysis meteorological data (1948–present), with a 2.5° resolution in both latitude and longitude (Kalnay et al., 1996). The back trajectories were started daily on an hourly basis at 500 m above the Renland elevation (71.305° N, 26.723° W; 2315 m a.s.l.) for the 17-year time span. The trajectory time was set to be 72 h, representing the average atmospheric lifetime of sea-salt aerosol (Lewis and Schwartz, 2004) and likely a lower limit for inorganic gas-phase bromine compounds. To access the potential marine sources of bromine and sodium, only a subset of the all trajectories is considered. Such selection limits the ensemble to only such trajectories that crossed the marine boundary layer (MBL), defined here as the 900 hPa isosurface (corresponding to approximately 1000 m a.s.l.), for at least 10 h. This pressure value was chosen according to Lewis and Schwartz (2004) and references within. One way to display a map of MBL crossings is the residence time analysis, a spatial distribution of trajectory end points (Ashbaugh et al., 1985). This map indicates that 75 % of the signal originates from the North Atlantic Ocean, extending in latitude from 50 to 85° N (up to the Fram Strait) and in longitude from the western coasts of Norway and the UK to east Greenland (Fig. 1), although the ocean regions closer to Renland are expected to be more significant as per the observed chemical signature. A minor contribution is expected from aerosols and gas-phase bromine originating from coastal waters off west Greenland. The consistency of sea ice reconstructions from the RECAP core and the Nordic Sea sediment cores (Sect. 4.2) suggests that the source area could extend to these regions throughout the last 90 kyr. For the

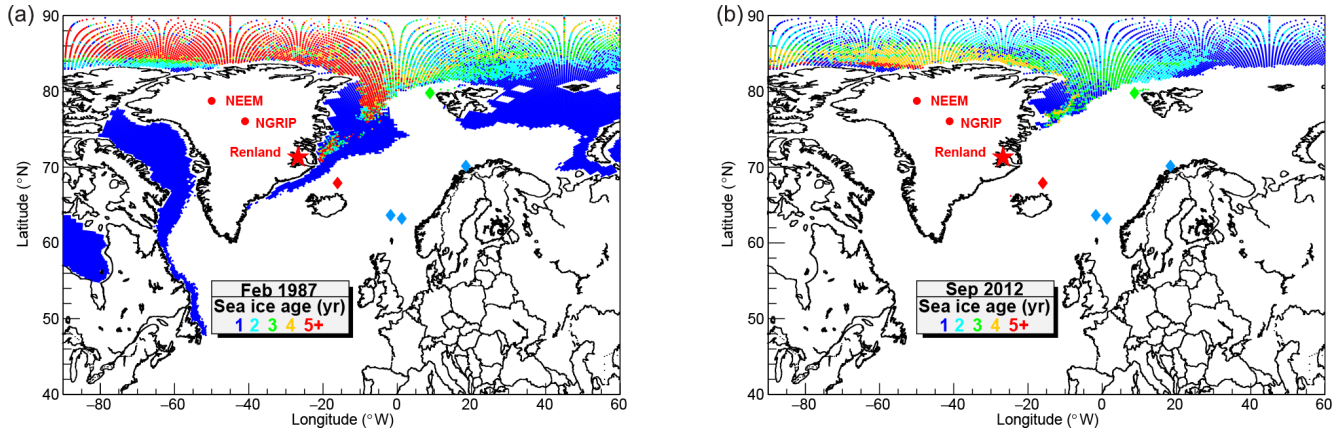

Figure 2. Map of modern Arctic sea ice age shown in representative extreme conditions: winter maximum (February 1987, **a**) and summer minimum (September 2012, **b**). The marine cores discussed in the text are indicated by coloured diamonds. See Fig. 1 for the marine core names and references. The sea ice age data are from NSIDC/NASA (v.3) (Tschudi et al., 2016).

overall interpretation of the RECAP record, the source area is therefore assumed to be the 75 % contour region of the residence time analysis end point distribution (Fig. 1). Such a region is nowadays mostly dominated by open-water (OW) conditions, with only minor contributions of FYSI grown in situ and multi-year sea ice (MYSI) transported south of the Arctic Ocean alongside the east Greenland coastline via the Transpolar Drift (Fig. 2).

3 Calculation of bromine enrichment (Br_{enr}) and Br_{enr} time series

The bromine enrichment values in the ice samples are calculated from the departure from the seawater abundance, the latter inferred from sodium (hereafter sea-salt sodium, ssNa), Eqs. (1), (2):

$$\mathrm{Br_{enr}} = \frac{\mathrm{Br/ssNa}}{(\mathrm{Br/Na})_m}, \quad (1)$$

$$\mathrm{Na} = \mathrm{ssNa} + \mathrm{nssNa}, \quad (2)$$

where Br, ssNa and nssNa are the bromine, sea-salt and non-sea-salt sodium concentrations in the ice samples respectively, and $(\mathrm{Br/Na})_m = 0.0062$ is the bromine-to-sodium mass ratio in seawater (Millero et al., 2008), assumed to be constant in time and space. Since sodium concentrations in ice cores can be interfered with by terrestrial inputs (nssNa, from sodium oxide Na_2O), which can generally contribute up to ≈ 10 %–50 % during glacial arid periods (i.e. stadials), nssNa and ssNa have to be evaluated to calculate Br_{enr} (Eqs. 1–2). We estimate the ssNa concentrations by using three methods. They make use of chlorine, magnesium and calcium concentrations.

The decrease in the Cl/Na mass ratio from the seawater reference (1.8 from Millero et al., 2008) can be related to extra sodium inputs of terrestrial origin. Thus, the ssNa can be calculated from chlorine if the measured chlorine-to-sodium ratio becomes less than 1.8, while zero nssNa is assumed otherwise (Eqs. 3–4):

$$\mathrm{ssNa} = \frac{\mathrm{Cl}}{1.8} \longleftrightarrow \frac{\mathrm{Cl}}{\mathrm{Na}} < 1.8, \quad (3)$$

$$\mathrm{ssNa} = \mathrm{Na} \longleftrightarrow \frac{\mathrm{Cl}}{\mathrm{Na}} \geq 1.8. \quad (4)$$

Unfortunately, sea-salt aerosols are affected by acid-scavenged (HNO_3 and H_2SO_4) dechlorination processes (e.g. $2NaCl + H_2SO_4 \rightarrow 2HCl + Na_2SO_4$), in which chlorine is removed as gas-phase HCl. These processes would increase the Cl/Na ratios in ice beyond the seawater reference (Legrand and Delmas, 1988), especially in warmer climatic conditions, since HCl is believed to have a longer atmospheric residence time than SSA. In fact, RECAP Holocene Cl/Na ratios (≈ 3) suggest that dechlorination processes do occur and chlorine is also deposited as HCl. Additionally, this result shows that HCl loss from the snowpack after deposition is limited, opposite to what is observed in Antarctica (Dome C) (Röthlisberger et al., 2003). The huge difference between Dome C and Renland accumulation rates likely explains such a polar asymmetry. In glacial ice, and especially during MIS 2 and MIS 4, the effect of dust neutralization of nitric and sulfuric acids would reduce chlorine loss both after deposition and during transport, therefore making the above correction more trustworthy (Wolff et al., 1995). However, the relative contributions of dechlorination processes and dust loading as per the observed Cl/Na ratios in the ice are difficult to quantify. A correction based on Cl/Na ratios was used by Hansson (1994) to calculate the ssNa and nssNa concentrations in the Renland core drilled in 1988. In particular, they found that nssNa accounts for respectively 17 % and 24 % of the total sodium during MIS 2 and MIS 4. If the same correction is applied to our measurements, we find values of 15 % and 20 %–30 % during MIS 2 and MIS 4.

A better alternative to calculate ssNa and nssNa would be to use an element of terrestrial origin. Magnesium contains both a marine and a terrestrial signature. By using reference mass ratios of Na/Mg in seawater and in the Earth upper continental crust, we are able to calculate the marine sodium contribution (Eq. 7). Often in ice core studies, the sea-salt and non-sea-salt contributions are calculated using global-mean reference values of the chemical composition of terrestrial elements (see for example Rudnick and Gao, 2003, Table 1). However, the spatial variability of the dust mineralogy can heavily impact the results. In our case, the terrestrial value $(Na/Mg)_t$ to be used in the calculation (the subscript "t" refers to "terrestrial") would require knowledge of the geochemical composition of the dust deposited at Renland. In remote Greenlandic ice cores, the provenance of aeolian mineral dust is believed to be the deserts in north-east Asia, as inferred from Sr, Nd and Pb isotopic ratios (Biscaye et al., 1997). We therefore carried out a compilation of present-day Na/Mg mass ratios of dust sourced from north-east Asian deserts, assuming that such an Asian dust source remained the dominant one over the last 120 kyr. For such analysis, the reader is referred to Appendix B, which considers $n = 6$ studies of dust composition (Na, Mg and Ca) from the Gobi and desert regions of Mongolian and from northern China deserts. This analysis (Appendix B) shows that, on average, dust from these regions exhibits the following ratios:

$$(Na/Mg)_t = 1.23, \quad (5)$$

$$(Na/Ca)_t = 0.38. \quad (6)$$

It is worth noting that these values differ substantially from global average values (Rudnick and Gao, 2003), especially for Na/Ca. By using the sodium-to-magnesium ratios in Asian dust $(Na/Mg)_t = 1.23$ (Eq. 5) and in seawater $(Mg/Na)_m = 0.12$ (Millero et al., 2008) (the subscript "m" refers to "marine"), we are able to calculate ssNa and ssMg (Eqs. 7–8):

$$ssNa = \frac{Na - (Na/Mg)_t \cdot Mg}{1 - (Mg/Na)_m \cdot (Na/Mg)_t}, \quad (7)$$

$$ssMg = \frac{(Mg/Na)_m \cdot Na - (Mg/Na)_m \cdot (Na/Mg)_t \cdot Mg}{1 - (Mg/Na)_m \cdot (Na/Mg)_t}. \quad (8)$$

In the Holocene, on average ssNa ≈ 0.99 Na, while ssMg $\approx$ 0.50–0.90 Mg. During MIS 2, ssNa ≈ 0.6–0.7 Na and ssMg ≈ 0.20–0.30 Mg, while during MIS 4 ssNa ≈ 0.50–0.60 Na and ssMg ≈ 0.10–0.20 Mg. In those Holocene samples where magnesium was not measured, we assume Na = ssNa, making on average a 1 % error.

The same procedure using calcium instead of magnesium has been applied to calculate ssNa concentrations from Antarctic ice cores (Röthlisberger et al., 2002), by solving the equations similar to Eqs. (7) and (8) with Mg replaced by Ca. In the RECAP record, such a correction using Asian dust $(Na/Ca)_t = 0.38$ and marine $(Ca/Na)_m =$ 0.038 (Millero et al., 2008) unrealistically predicts ssNa ≈ 0 throughout the glacial period. Small changes in the $(Na/Ca)_t$ value do not significantly change this result. It appears that higher than expected calcium is deposited at Renland, and therefore a lower $(Na/Ca)_t$ is to be used. The excess of calcium during the glacial period has been reported in Greenlandic ice cores, in the form of calcite ($CaCO_3$), dolomite ($CaMg(CO_3)_2$) and gypsum ($CaSO_4 \cdot 2H_2O$) minerals (Mayewski et al., 1994; Maggi, 1997; De Angelis et al., 1997). In their investigation of the GRIP ice core Legrand and Mayewski (1997) find a larger increase in sulfate (SO_4^{2-}) in Greenland compared to Antarctica during glacial times. Such large enhancements of the sulfate level are well correlated with calcium increases but not with MSA, suggesting that sulfate levels are related to non-biogenic sulfur sources (gypsum emissions from deserts, for instance) (Legrand and Mayewski, 1997). Different calcium sources were likely active during the glacial period as compared to warmer periods, but it is unclear whether these were new active continental sources or continental shelves which became exposed due to a lowered sea level. Similarly to what has been observed in other Greenland ice cores, extra calcium is also found in the RECAP core during the glacial, as illustrated from the scatter plot with magnesium (Fig. 3). From this calcium–magnesium relation, we estimate that during the coldest and most arid glacial times $(Ca/Mg)_t = 23 \pm 1$ (blue fit in Fig. 3), while in other periods we assume that the composition remained the same as the modern Asian dust composition (Appendix B):

$$\left(\frac{Ca}{Mg}\right)_{t,modern} = 3.7. \quad (9)$$

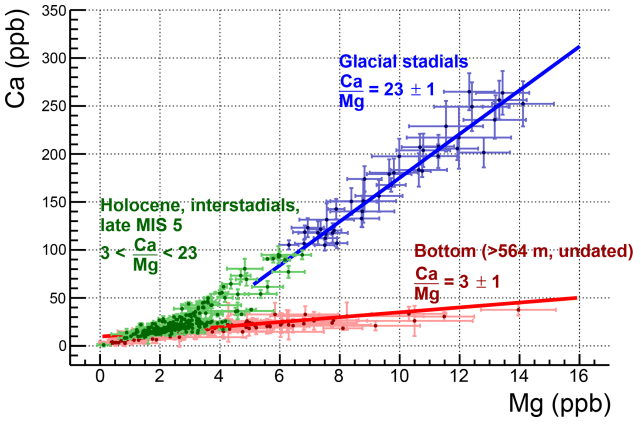

Figure 3. Calcium and magnesium concentrations in the RECAP core. Samples with high (> 100 ppb) calcium concentrations are drawn in blue. The red samples of the bottom 22 m (562–584 m depth) are not dated but may consist of Eemian ice (see main text). All others samples are drawn in green. The Ca/Mg ratio varies between 3 ± 1 (Asian dust) and 23 ± 1 (gypsum and/or excess of carbonate). The seawater ratio $(Ca/Na)_m = 0.32$ cannot be identified.

This hypothesis is substantiated by the value found for the lower envelope for the Holocene, interstadial late MIS 5 samples (green points in Fig. 3) as well as for composition of the bottom 22 m of the core (562–584 m, red points in Fig. 3): $(Ca/Mg)_t = 3 \pm 1$ (red fit). We note that these bottom measurements do not appear in any time series since the core chronology ends at 120 ka (562 m). We therefore here suggest that the RECAP bottom 22 m date back to the previous interglacial, the Eemian.

Sea-salt sodium concentrations (ssNa) can therefore be calculated using calcium, by replacing Mg→Ca in Eq. (7) and by using $(Ca/Na)_m = 0.038$ and $(Na/Ca)_t$ calculated by

$$\left(\frac{Na}{Ca}\right)_t = \frac{(Na/Mg)_{t,modern}}{(Ca/Mg)_{t,\ glacial\ fit}} = \frac{1.23}{23} = 0.054. \quad (10)$$

As a comparison, in the GRIP core, where the ssNa calculations were based on a mixed chlorine–calcium method, De Angelis et al. (1997) found empirically that $(Na/Ca)_{t,glacial} = 0.036$ in glacial ice (significant correlation, $\rho = 0.7$) and $(Na/Ca)_{t,modern} = 0.07$ (weak correlation, $\rho = 0.2$) in Holocene ice.

The calculation of RECAP nssCa reveals that calcium contains almost a purely crustal signature: nssCa $\gtrsim$0.95Ca throughout the record.

The ssNa curves calculated with magnesium and calcium ($ssNa_{Mg}$, $ssNa_{Ca}$) differ by less than 1σ, while appreciable differences between these two curves and the chlorine one ($ssNa_{Cl}$) are only found during MIS 2 and MIS 4 (Fig. 4b). A weak positive correlation ($\rho = 0.32$, $p < 10^4$, $n = 144$) is found between Br and $ssNa_{Mg}$ concentrations in glacial ice (Appendix C, Fig. C1) suggesting that although the two elements share a common marine source, other source or transport effects are playing a role in driving changes in their respective ice concentrations.

Since $ssNa_{Mg} \simeq ssNa_{Ca}$, for the following discussion we will only consider the two Br_{enr} series based on the chlorine and magnesium calculation: $Br_{enr,Cl}$ and $Br_{enr,Mg}$ (Fig. 4g). Standard error propagation is carried out to yield the final Br_{enr} uncertainties.

This analysis along with past studies demonstrate that the sea-salt and non-sea-salt calculations of elemental concentrations depend on the chemical composition of the dust that is deposited at the ice core site. The dust composition has a spatial variability which should be considered, while the use of tabulated reference values should be discouraged.

From the two calculated RECAP Br_{enr} curves ($Br_{enr,Cl}$, $Br_{enr,Mg}$), we now investigate past sea ice conditions in the 50–85° N North Atlantic Ocean, based on the aforementioned hypotheses on the Br_{enr} use as an indicator of first-year sea ice conditions. Because of the RECAP location, the record is sensitive to ocean processes and sea ice dynamics (Cuevas et al., 2018; Corella et al., 2019). We compare our sea ice record with PIP_{25} results from five marine sediment cores drilled within the Renland source area: the Fram Strait, the Norwegian Sea and the North Icelandic shelf. The PIP_{25} index is a semi-quantitative indicator of the local sea ice conditions at the marine core location. It is calculated by coupling the sediment concentration of IP_{25}, a biomarker produced by diatoms living in seasonal sea ice, with an open-water phytoplankton biomarker (brassicasterol or dinosterol, hence P_BIP_{25} or P_DIP_{25}). Briefly, the PIP_{25} index is a dimensionless number varying from 0 to 1: $PIP_{25} \approx 1$ indicates perennial sea ice cover; $PIP_{25} \approx 0$ indicates open-water conditions, while intermediate PIP_{25} values reflect seasonal sea ice (Müller et al., 2011; Belt and Müller, 2013).

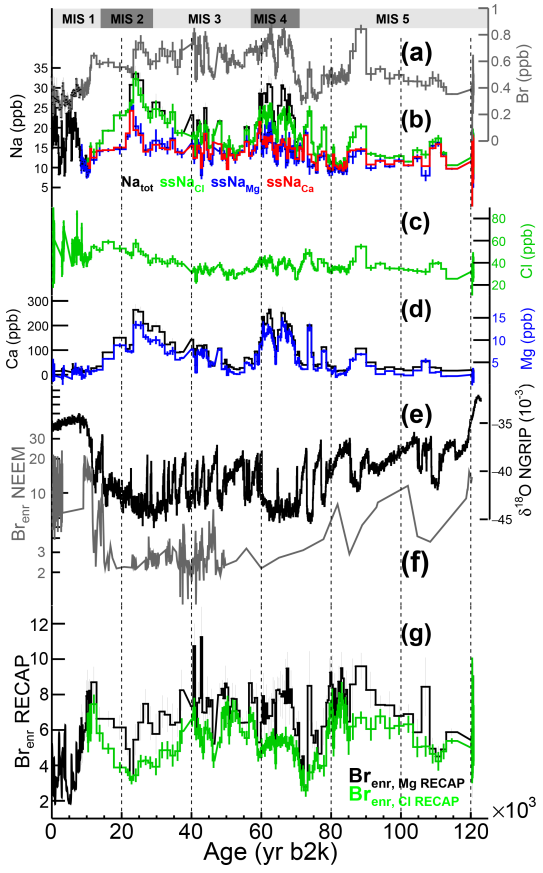

Figure 4. The 120 kyr time series of analyte concentrations in the RECAP ice core. The last 8 kyr are 100-year averages. **(a)** bromine; **(b)** total sodium and sea-salt sodium (ssNa) series calculated using chlorine (green), magnesium (blue) and calcium (red); **(c)** chlorine; **(d)** calcium (black) and magnesium (blue); **(e)** NGRIP $\delta^{18}O$ from North Greenland Ice Core Project members (2004); **(f)** NEEM Br_{enr} from Spolaor et al. (2016b); **(g)** RECAP Br_{enr} series ($Br_{enr,Cl}$, green and $Br_{enr,Mg}$, black) calculated using chlorine and magnesium respectively.

4 Results and discussion

The two Br_{enr} time series ($Br_{enr,Cl}$ and $Br_{enr,Mg}$), based on either chlorine or magnesium for the sea-salt sodium calculation, display values greater than 1 throughout the record,

suggesting an FYSI signature throughout the last 120 kyr in the North Atlantic (Fig. 4g). The very low values found in the Holocene (on average $Br_{enr,Hol} = 3.9$, rms (root mean square) $= 1.5$) suggest minimum FYSI during the current interglacial. Although the record does not extend to the Eemian period, it shows that at the inception of the last glacial period, $\sim 120\,000$ years ago, Br_{enr} values were higher than in the Holocene (on average $Br_{enr,120\,kyr} = 5.4$, rms $= 1.1$, $n = 38$), suggesting that more FYSI was present at that time. From 120 kyr ago the Br_{enr} levels increased until the Greenland Interstadial 21 (GI-21), ~ 85–80 kyr ago ($Br_{enr,85-80\,kyr} \simeq 8$). Hereafter, they decreased throughout late MIS 5. From late MIS 5 to MIS 4, rising Br_{enr} values are observed, but a statistically significant difference between the two Br_{enr} curves results from the two ssNa corrections, with the $Br_{enr,Mg}$ series showing higher values than $Br_{enr,Cl}$. The two series converge again at the beginning of MIS 3, with values around 7 ± 1. From ~ 50–40 ka, both series start to decrease. The decrease is more significant for $Br_{enr,Cl}$. Minimum Br_{enr} values are reached at the Last Glacial Maximum during MIS 2. The deglaciation reveals a Br_{enr} increase up to ca. 12 000 years ago, followed by a steady decrease towards the Holocene.

The first Arctic glacial–interglacial investigation of Br_{enr} was performed on the NEEM ice core, located in northwest Greenland. At NEEM, the main source regions for sea-ice-related processes are believed to the Canadian archipelago, the Baffin Bay and the Hudson Bay (Spolaor et al., 2016b; Schüpbach et al., 2018). The 120 000-year NEEM record (Spolaor et al., 2016b) showed higher Br_{enr} values during the Holocene and interstadials compared to the glacial stadials (Fig. 4f). This was interpreted as greater FYSI conditions existing during such warmer periods, while the lower Br_{enr} values during colder climate phases would indicate more extended MYSI coverage in those ocean regions. In accordance with their respective source regions, the Br_{enr} record from the NEEM ice core is markedly different from the RECAP one (Fig. 4). In the NEEM core, Br_{enr} was positively correlated to $\delta^{18}O$ throughout the entire climatic record. In contrast, at Renland, such a consistent correlation is not present, and Br_{enr} is at times lower during warmer climate periods (e.g. during the Holocene). We suggest that this difference originates from the fact that during warm periods, the relative FYSI-to-OW influence is greater at NEEM than at Renland, the latter being mostly dominated by OW conditions in the North Atlantic. This is supported, at least for present conditions, by a model study that investigated the Arctic spatial variability of the ratio of sea ice to open-ocean sodium loadings (Rhodes et al., 2018), where it was found that such ratio at NEEM is ~ 5 times higher than Renland.

Since the increase in atmospheric bromine is believed to reflect the strength of bromine recycling from FYSI surfaces, low values of Br_{enr} could indicate either OW or MYSI conditions. Thus, we suggest that Br_{enr} is a signature, at Renland, of contrasting sea ice states: FYSI/MYSI and FYSI/OW. We also suggest that the former (FYSI/MYSI) occurs during generally colder periods while the latter (FYSI/OW) occurs during generally warmer periods. In the framework of this dual regime behaviour, if the ice core time resolution is high enough, an increase in Br_{enr} values followed by a maximum and a negative trend should be a signature of an ocean facing gradual changes from open ocean to multi-year sea ice conditions, or vice versa, in the case of monotonically warming or cooling ocean temperatures (Fig. 5). One such regime shift is observed in the RECAP Br_{enr} record during the deglaciation (Fig. 4g). At the Last Glacial Maximum (LGM, ~ 23 ka), the low enrichment values ($Br_{enr,Mg,LGM} = 3.3 \pm 0.3$; $Br_{enr,Cl,LGM} = 3.2 \pm 0.2$) suggest reduced FYSI recycling and therefore extensive MYSI conditions (blue arrow in Fig. 5; OW conditions are considered unlikely). Transitioning from the Last Glacial Maximum into the Holocene, Br_{enr} increases until ~ 12 ka ($Br_{enr,Mg,12\,kyr} = 8.7 \pm 0.9$; $Br_{enr,Cl,12\,kyr} = 7.5 \pm 0.5$), indicating maximum FYSI at this time (Figs. 4 and 6). Hereafter, a decrease is observed, as Br_{enr} continues to drop during the Early Holocene and the proxy operates in the FYSI/OW regime (red arrow in Fig. 5).

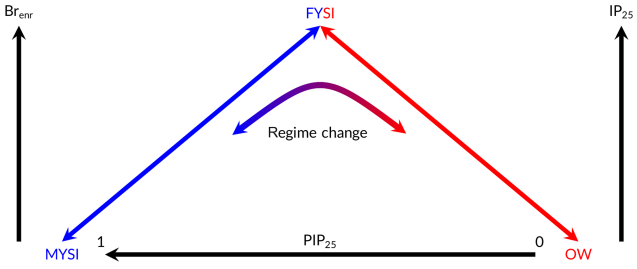

Figure 5. Schematic illustration of marine and (suggested) ice-core-based sea ice indicators as a function of different sea ice conditions. Br_{enr} (ice core) and IP_{25} (sediment core) increase as a function of first-year sea ice (FYSI) area. Low values can thus indicate either open-water (OW) or multi-year sea ice (MYSI) conditions, depending on the climate state. The PIP_{25} index is a marine-derived semi-quantitative indicator of local sea ice conditions at the marine core location. $PIP_{25} \sim 0$ ($PIP_{25} \sim 1$) indicates open-water (perennial sea ice, i.e. MYSI) conditions, while intermediate PIP_{25} values reflect seasonal sea ice (i.e. FYSI). Br_{enr} values in the RECAP core are believed to indicate an FYSI/OW regime in a "warm" climate state and an FYSI/MYSI in a "cold" climate state.

4.1 The last deglaciation and the dual Br_{enr} regimes

We now consider in further detail the last deglaciation, when a number of ocean temperature, salinity, circulation and sea ice changes are observed in the Nordic Seas (Fig. 6). Marine-derived local sea ice records from both the Svalbard margin and the Norwegian Sea indicate (Fig. 6e, f) that near-perennial sea ice ($PIP_{25} \approx 0.5$–1) was present during MIS 2 until ~ 17 ka (17.6 ka recorded in the Svalbard margin), the onset of a major break-up of extensive sea ice cover, during Heinrich Event 1 (18 to 15 ka). Synchronous to within a few centuries, several modifications relevant to the North

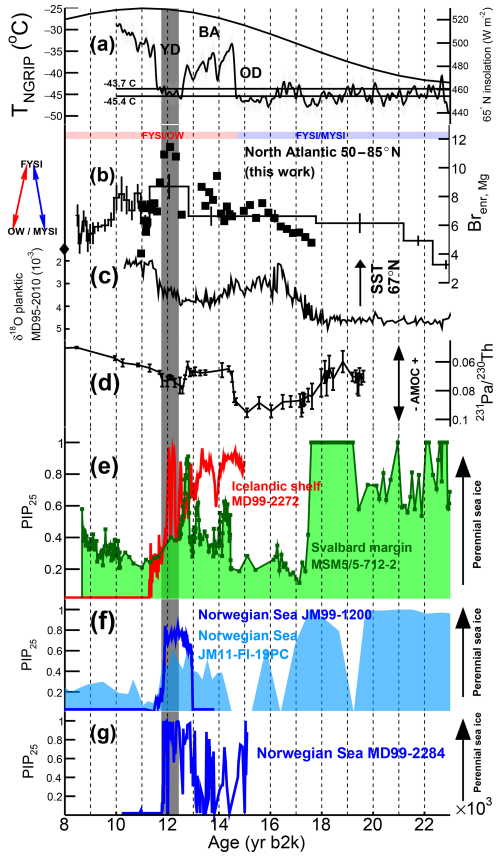

Figure 6. Climate records during the last deglaciation. **(a)** NGRIP air temperature reconstruction (Kindler et al., 2014) ($\pm 1\sigma$ = 2.5 °C). The two horizontal lines correspond to a $\pm 2\sigma$ deviation from the mean temperature (−44.6 °C) found during the 12.4–11.8 ka period of maximum $Br_{enr,Mg}$ (grey vertical band). The T_{NGRIP} record does not extend before 10 ka but the temperature is not expected to cross the threshold at any time in the Holocene. The black line is the 21 June daily mean insolation at 65° N (Laskar et al., 2004). **(b)** RECAP $Br_{enr,Mg}$ (thick black line) and repeat sampling conducted at higher resolution (squares). Since for the highly resolved measurements magnesium was not measured, for the calculation of the sea-salt sodium concentrations and the $Br_{enr,Mg}$ values (Eqs. 1–7) we used the magnesium values of the four low-resolution samples. Over the time period covered by the repeat measurements, nssNa $\simeq$ 10 %–20 %. The average $Br_{enr,Mg}$ value measured during the Holocene is indicated by a diamond. **(c)** Planktonic $\delta^{18}O$ record from sediment core MD95-2010 (66°41.05′ N, 04°33.97′ E, from Dokken and Jansen, 1999). Lower $\delta^{18}O$ values indicate warmer and fresher ocean waters. **(d)** Record of $^{231}Pa/^{230}Th$ ratios within a sediment core retrieved in the deep western subtropical Atlantic (33°42′ N, 57°35′ W). Sedimentary $^{231}Pa/^{230}Th$ are believed to reflect Atlantic meridional overturning circulation (AMOC) strength (McManus et al., 2004). **(e, f, g)** PIP_{25} records from the Svalbard margin (green, core MSM5/5-712-2, Müller and Stein, 2014), the North Icelandic shelf (red, core MD99-2272, Xiao et al., 2017) and the Norwegian Sea (core JM11-FI-19PC from Hoff et al., 2016); core JM99-1200 from Cabedo-Sanz et al. (2013); and core MD99-2284 from Muschitiello et al. (2019). The PIP_{25} scale varies from perennial sea ice ($PIP_{25} \approx 1$) to open-water ($PIP_{25} \approx 0$) conditions (see Fig. 5). See Fig. 1 for the PIP_{25} core locations.

Atlantic Ocean are observed (Fig. 6), including seawater surface freshening and warming in the polar and subpolar North Atlantic (the 67° N Dokken and Jansen, 1999, record is shown as an example in Fig. 6c) and a near total cessation of the Atlantic Meridional Overturning Circulation (AMOC; Fig. 6d). Generally low to intermediate PIP_{25} values ($PIP_{25} \approx 0$–0.5) are reported in the Svalbard Margin and in the Norwegian Sea in the $\sim$ 17–12 ka period (Fig. 6e, f, g), with a slight increasing trend throughout the Bølling–Allerød (BA) and a broad maximum reached during the Younger Dryas (YD), suggesting that seasonal sea ice conditions were dominating this period. Other studies from marine records in the Nordic Seas records also suggest milder sea ice conditions during the BA and increased sea ice during the YD (Belt et al., 2015; Cabedo-Sanz et al., 2016). In contrast, a record from the North Icelandic shelf (Fig. 6e) shows that here the sea ice conditions remained near-perennial from 14.7 to 11.7 ka ($PIP_{25} \approx 0.5$–1). The authors (Xiao et al., 2017) suggest that this pattern of more severe sea ice conditions in the north of Iceland is, at least during the BA and the YD, linked to the flow of warmer waters from the North Atlantic Current, influencing sea ice melting in the eastern Nordic Seas, whereas the Icelandic shelf is influenced by colder polar waters from the East Greenland Current and the East Icelandic Current.

The RECAP ice core was resampled at a sub-centennial resolution to better constrain the timing of sea ice changes through the deglaciation in the 50–85° N North Atlantic (Fig. 6b, squares). The $Br_{enr,Mg}$ series ($Br_{enr,Cl}$ would lead to the same results) would indicate that FYSI started to increase in the North Atlantic, concurrent with a reduction in MYSI, at $\sim$ 17.5 ka, synchronous with a local PIP_{25} decrease in the Svalbard margin and eastern Nordic Seas and in response to sea surface temperature warming in the North Atlantic. This finding would also suggest that North Atlantic sea ice changes occurred in concert with temperature and circulation changes in the underlying surface waters. We note that this time period also coincides with the initiation of deglacial changes in mean ocean temperature, Antarctic temperatures and atmospheric CO_2 concentrations toward interglacial values (Bereiter et al., 2018). North Atlantic FYSI continued to increase throughout the BA (except for one point at 12.7–12.4 ka at the onset of the YD) until a maximum at 12.4–11.8 ka during the YD, when a clear $Br_{enr,Mg}$ maximum is observed (Fig. 6b). From the comparison between the marine and ice core results, we infer that, during the 17–12 ka period, the 50–85° N-integrated North Atlantic sea ice changed from MYSI to FYSI. Local sea ice was also melting at $\sim$ 17 ka in the eastern Nordic Seas, likely influenced by the North Atlantic Current, while, at least from 14.7 to 11.7 ka, sea ice was still near-perennial at the North Icelandic shelf, possibly due to the influence of cold waters carried by the East Greenland Current. Following its maximum value at 12.4–11.8 ka, Br_{enr} (i.e. FYSI) started to decrease (Fig. 6b). We suggest that from this point in time, the Br_{enr} indicator now shifts to

the FYSI/OW regime (Fig. 5), and the North Atlantic basin becomes largely ice free. A retreating FYSI scenario is also recorded in all five marine cores (decreasing PIP_{25} to ≈ 0–0.4 during the Early Holocene; Fig. 6e, f, g), suggesting that open-water conditions progressively developed in the whole North Atlantic basin, sustained by increasing heat transport from the North Atlantic Current and a strengthened AMOC since $\sim$ 11.7 ka (McManus et al., 2004; Ritz et al., 2013).

Since Br_{enr} is assumed to be an increasing function of FYSI, its decrease would point to either OW or MYSI conditions, following either the FYSI/OW or the FYSI/MYSI regimes (Fig. 5). At any point in time, only one regime is considered to be in place, and we suggest a simple model in which a temperature threshold could be the discriminating variable setting the regime type. Since a change in regime is observed during the deglaciation, with maximum Br_{enr} values (i.e. FYSI) at 11.8–12.4 ka, we set the threshold to be the mean NGRIP ice core temperature reconstructed for that period: $T_{NGRIP} = -44.6 \pm 0.9\ (2\sigma)\ °C$ (the two lines in Fig. 6a). In every ice sample of the 120 000-year record the regime type (FYSI/MYSI or FYSI/OW; Fig. 5) can thus be determined according to its integrated temperature value with respect to the temperature threshold: FYSI/MYSI for a lower temperature value and FYSI/OW for a higher temperature value.

According to this simple model the deglaciation is characterized by the FYSI/MYSI regime until the onset of the Bølling–Allerød (except few points at which the regime type depends on the chosen threshold value; Sect. 4.2), while the FYSI/OW regime operated from that point forward. We note that there is no similar Br_{enr} maximum at the onset of the Bølling–Allerød as seen in the YD at the point when NGRIP temperature is crossing the same temperature as found in the YD. The possible explanation of higher Br_{enr} values during the Younger Dryas compared to the Bølling–Allerød may reside in the higher seasonal temperature variations (Buizert et al., 2014) and freshwater inputs from melting ice sheets in the former period, both promoting the formation of seasonal sea ice. Conversely, the lower Br_{enr} values (hence to greater MYSI in the FYSI/MYSI regime) during the Older Dryas compared to the Bølling–Allerød and the Younger Dryas may be linked to the overall much lower temperatures during this period (Buizert et al., 2014), higher surface water salinity due to less freshwater inputs from melting ice sheets and a generally weaker AMOC. It appears that the NGRIP temperature threshold alone is unable to fully represent the suggested two-regime modelization during the deglaciation, possibly due to concomitant changes in other sea-ice-related climate variables during this period. We suggest that at glacial–interglacial timescales such a temperature-based discrimination could be still used to represent the two-regime variability.

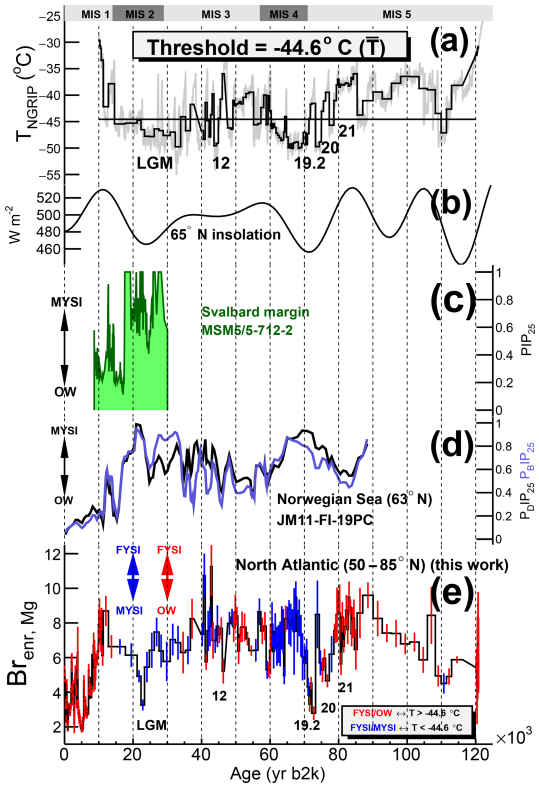

Figure 7. Discrimination between the two $Br_{enr,Mg}$ regimes according to the −44.6 °C NGRIP temperature threshold and North Atlantic sea ice records from marine cores. **(a)** Reconstructed NGRIP temperature (grey; Kindler et al., 2014). The temperature threshold value is the mean temperature during the 11.8–12.4 ka period, when the change in $Br_{enr,Mg}$ regime was observed (see Fig. 6). The black series is the NGRIP temperature profile downscaled to the measured Br_{enr} resolution. The numbers indicate the Greenland Interstadials (GIs) discussed in the text. **(b)** Daily mean insolation on 21 June at 65° N (Laskar et al., 2004). **(c)** PIP_{25} record from the Svalbard margin (core MSM5/5-712-2 from Müller and Stein, 2014). **(d)** P_DIP_{25} and P_BIP_{25} 90 kyr records from the Norwegian Sea presented as five-point running mean (from Hoff et al., 2016). **(e)** Discrimination between the $Br_{enr,Mg}$ regimes computed according to the integrated temperature value with respect to the threshold. The FYSI/OW and FYSI/MYSI regimes are indicated with red and blue error bars respectively.

4.2 The 120 000-year Br_{enr} record

We now apply the previously mentioned temperature-based discrimination between the two sea ice regimes to the 120 000-year $Br_{enr,Mg}$ record (Fig. 7). The regime type in each ice sample is represented by the colour of the error bars: blue for the FYSI/MYSI regime and red for the FYSI/OW regime. In order to test the sensitivity of the regime output to the threshold value, four scenarios are computed, using a $\pm 1\sigma$ and a $\pm 2\sigma$ value around the temperature threshold mean value $\overline{T} = -44.6\,°C$ (Fig. D1). Except for 2(1) samples at ca. 20 ka showing a different regime type in the $\overline{T}$-

2(1)σ scenario during the deglaciation (Fig. D1), the regime discrimination mentioned in the following discussion is invariant with respect to the four temperature-based scenarios. The same analysis is also performed on the $Br_{enr,Cl}$ curves (Fig. D2).

MIS 5 is characterized by increasing $Br_{enr,Mg}$ values in the FYSI/OW regime from 120 to 80 kyr ago (Greenland Interstadial, GI-21, Fig. 7). We interpret this trend with increasing FYSI extent in the North Atlantic. From the end of GI-21 the Br_{enr} regime changes to FYSI/MYSI as the NGRIP temperature drops during late MIS 5 and MIS 4. As compared to the levels reached during GI-21 (8 ± 1), lower $Br_{enr,Mg}$ values are found during GS-21, GS-20 and GS-19 (5 ± 2) and on average during MIS 4 (7 ± 1). We interpret the combined effect of decreased $Br_{enr,Mg}$ values in the FYSI/MYSI regime with an increase in MYSI extent in the North Atlantic from late MIS 5 to MIS 4. The $Br_{enr,Cl}$ curve shows even lower values during MIS 4, predicting more extended MYSI than the $Br_{enr,Mg}$ record (Fig. D2). Overall, from 120 kyr ago to MIS 4, the change in Br_{enr} regime (from FYSI/OW to FYSI/MYSI) is opposite to what is observed during the deglaciation (from FYSI/MYSI to FYSI/OW): from a relatively warm climate 120 kyr ago, the cooling trend is characterized by an increasing FYSI extent until the point (GI-21) at which the FYSI starts to be replaced by MYSI. This maximum $Br_{enr,Mg}$ value at the time of the regime change (GI-21) is similar to the peak $Br_{enr,Mg}$ value reached during the deglaciation: $Br_{enr,Mg}(12\,kyr) \simeq Br_{enr,Mg}(GI\text{-}21) \simeq 8$. The same result holds if one considers the $Br_{enr,Cl}$ series (Fig. D2). Unlike the longer lasting GI-21, the Greenland Interstadials GI-20 and GI-19.2 display very low Br_{enr} values ($\simeq$ 3–5). A possible explanation for these low values could be found in a fast replacement (at least not captured by the time resolution of the Br_{enr} record) of MYSI by OW conditions. Higher time-resolved measurements would be needed to test this hypothesis.

Moving from MIS 4 to MIS 3, the $Br_{enr,Mg}$ values remain within 1σ of each other. This suggests a similar FYSI extent in the two periods, although the FYSI/MYSI regime operating during MIS 4 could suggest an extra MYSI extent during this period, as compared to MIS 3, the latter being generally characterized by a mixture of both Br_{enr} regimes. This hypothesis is supported by the $Br_{enr,Cl}$ series, which shows lower values during MIS 4 than MIS 3 (Fig. D2). A sea ice record in the Norwegian Sea (Hoff et al., 2016) also indicates more perennial sea ice conditions during MIS 4 than during MIS 3. The time resolution does not allow a deep investigation of DO events during MIS 3, although a low Br_{enr} value in the FYSI/OW regime during the GI-12 ($Br_{enr,Mg}$(46.0–46.6 ka) $= 5.2 \pm 0.7$) suggests a shift to open-water conditions during this interstadial, similarly to GI-19.2 and GI-20. Possibly, similar sea ice dynamics were in play during these stadial–interstadial transitions. Increased time resolution is, however, needed to better characterize DO events.

MIS 2 is characterized by an FYSI/MYSI regime and progressively decreasing $Br_{enr,Mg}$ values (Fig. 7e), with a minimum being reached $\sim$ 23 kyr ago, during the Last Glacial Maximum: $Br_{enr,Mg}(LGM) = 3.3 \pm 0.3$. We interpret this negative $Br_{enr,Mg}$ (and $Br_{enr,Cl}$, Fig. D2) trend with progressively increasing MYSI conditions in the whole North Atlantic, which reached a maximum during the LGM. Relatively high and increasing PIP_{25} values ($\approx$ 0.5–1) are found in the Norwegian Sea record (Fig. 7d), with maximum sea ice registered ca. 20–23 kyr ago. The sea ice record from Fram Strait is in broad agreement with the Norwegian record, the former showing high ($\approx$ 0.5–1) and variable PIP_{25} values until the longer lasting 19 ka maximum (Fig. 7c). Overall, the cold MIS 2 period is characterized by decreasing seasonal sea ice and increasing multi-year sea ice across the North Atlantic, with a maximum reached ca. 20 kyr ago.

The deglaciation is characterized by increasing FYSI conditions until the mid-Younger Dryas (12.4–11.8 kyr ago), followed by a return to the FYSI/OW regime and decreasing Br_{enr} values as open waters progressively replaced sea ice in the Holocene. A clear sea ice decline is also reported in the Norwegian Sea following the LGM towards the current interglacial (Figs. 6 and 7).

5 Conclusions and outlook

We present a 120 000-year record of bromine enrichment (Br_{enr}) from the RECAP ice core and interpret it in terms of FYSI variability in the 50–85° N-integrated North Atlantic Ocean. The record suggests that, during the last deglaciation, sea ice started to transform from multi-year to first-year $\sim$ 17.5 kyr ago, probably triggered by increasing surface ocean water temperatures. Increasing first-year sea ice conditions are observed throughout the Older Dryas, the Bølling–Allerød and the Younger Dryas. During these periods, the availability of freshwater from melting ice sheets, seasonal temperature variations and AMOC strength likely played a role in driving the sea ice changes. The maximum first-year sea ice signature is found 12.4–11.8 kyr ago, during the Younger Dryas, whereupon open ocean was the dominant condition during the Holocene (MIS 1). Although the RECAP sea ice record does not extend back to the warmest period of MIS 5, it does show that sea ice extent during the Holocene is lower than at any time in the past 120 000 years. Minimum first-year sea ice, likely associated with maximum multi-year sea ice conditions existed during MIS 2 and possibly during MIS 4. Compared to MIS 2, greater first-year sea ice extent existed during MIS 3 and MIS 5. Increased time resolution is needed to fully resolve Dansgaard–Oeschger oscillations. However, the data indicate that during GI-12, GI-19.2 and GI-20, large extent of first-year sea ice could have been replaced by open ocean, while large first-year sea ice areas existed during GI-21.

These analyses and conclusions rely on a number of hypotheses and assumptions mainly concerning the validity of Br_{enr} as a proxy for first-year sea ice. Efforts are still needed in the direction of validating these assumption and investigating the limitations and processes that affect the Br_{enr} signature in present deposition and in old ice core records.

Data availability. The RECAP ice core data will be made available on NOAA paleoclimate and PANGAEA online data archives.

Appendix A: Bromine loss from the snowpack

The stability of bromine after deposition has been questioned since the first investigation carried out by Dibb et al. (2010) in Summit (Greenland). We summarize here the experimental investigations that have been carried out on this topic ever since both in Antarctica and in the Arctic.

A1 Antarctica

McConnell et al. (2017) investigated simultaneous sodium and bromine fluxes across Antarctica (see their Fig. S4 in the Appendix showing the reconstructed fluxes from an array of 11 cores measured in McConnell et al., 2014). In particular, the J(Na) and J(Br)–accumulation rate (A) linear relations (impressive J(Br)–A linear fit from 50 to 400 kg m^{-2} yr^{-1}) suggest that, while sodium loss is negligible, bromine re-emission is quantified to 17 ± 2 µg m^{-2} yr^{-1} (negative intercept, i.e. snow–air flux). According to the results, the bromine loss from Antarctic snowpack would be 65 % at sites with $A = 50$ kg m^{-2} yr^{-1}, 32 % at sites with $A = 100$ kg m^{-2} yr^{-1}, 22 % at sites with $A = 150$ kg m^{-2} yr^{-1}, 16 % at sites with $A = 200$ kg m^{-2} yr^{-1}, 13 % at sites with $A = 250$ kg m^{-2} yr^{-1} and 11 % at sites with $A = 300$ kg m^{-2} yr^{-1} (note that this exercise works on the hypothesis that the bromine air concentration is the same above all sites, but the goodness of their fit would suggest that this is the case). These negative fluxes would be representative of Antarctic conditions for the duration of the records, i.e. few centuries to 2 millennia maximum (see Supplement Table S2 in the 2014 ref). In their Dome C ($A = 30$ kg m^{-2} yr^{-1}) study, Legrand et al. (2016) analysed bromine content in a 110 cm deep, 2 cm resolution snow pit. Their measurements show that the upper 2 cm contain 1.25 times more bromine that the 2–4 cm layer, 2.5 times more than the 4–8 cm layer and ca. 10 times more than the 8–12 cm layer. Based on the higher bromine concentrations towards the surface the authors suggest a possible bromine remobilization from the snow. In testing the hypothesis, the authors model whether the measured bromine snow content is high enough to sustain the 1.7 pptv air concentration of Br_y they measured in the overlying atmosphere. They find that to explain such a value, the snow bromine storage should be 35 times larger than the actual measurements. They therefore conclude that in Dome C their investigation do not support the importance of snowpack bromine emissions. This conclusion contrasts with what would be concluded by McConnell and co-workers.

From a surface snow experiments carried out in Dome C in 2014 (Antarctica, $A = 30$ kg m^{-2} yr^{-1}) by Spolaor et al. (2018), the authors observe constant bromine concentrations from mid-December to mid-January (austral summer). In a similar experiment carried out the following year, from late November to late December 2015, higher bromine concentrations were found in November (late spring) with a decreasing trend towards the end of the year. The authors relate such a drop to a change in the source of the air masses, from coastal to inland, as inferred from back trajectory modelling, rather than to bromine loss from the snow.

From another surface snow experiment carried out at GV7 (Antarctica, $A = 270$ kg m^{-2} yr^{-1}), Vallelonga et al. (QSR, 2019) compare bromine fresh surface snow concentrations with snow pit values and suggest, on the basis of similar values between the values in the surface samples and in the surface of the snow pit (that would integrate the values of the surface samples), that at this site bromine is stable after deposition (the McConnell calculation would predict a loss of 12 %). Looking at the 100–300 µg m^{-2} yr^{-1} annual bromine (2010, 2011, 2012, 2013) fluxes calculated along the Talos Dome–GV7 traverse (Maffezzoli et al., 2017), a negative flux of 17 ± 2 µg m^{-2} yr^{-1} would imply that, if present, the bromine loss can be quantified in this region as 6 %–17 %. As McConnell and co-workers point out, it is surprising that the snow–air bromine flux they found is not dependent on snow accumulation (their fit appears linear until the last point: 400 kg m^{-2} yr^{-1}).

A2 Arctic

In the Arctic, the most robust piece of evidence results from hourly resolved surface snow measurements carried out in coastal Svalbard, showing that bromine photolytic loss cannot be appreciated across night–day cycles (Spolaor et al., 2019; see Fig. 6).

In an experiment described in QSR (2019) that Vallelonga and co-workers carried out in Ny-Ålesund (Svalbard, $A = 600$ kg m^{-2} yr^{-1}), sodium and bromine were measured in surface snow daily from April to June (spring to summer). From April to late May Br_{enr} values decreased by a factor of 2 (max) (afterwards surface melting and positive temperatures led to 80 % sodium drainage from the snowpack). It is difficult, however, to determine whether this decrease is due to bromine re-emission or to early spring bromine explosions from sea ice surfaces, located ca. 150 km away from the sampling site, enriching the spring deposited snow layers.

A3 Conclusive remarks on bromine loss

To conclude, field experiments aimed at quantifying bromine loss from the snowpack are made difficult by the concurrent effect of other variables (source effects, changes in transport pathways, other postdepositional processes) that can act simultaneously. Estimates of bromine loss from Dome C (Antarctica) have not led to unique conclusions. This site is likely one of the most challenging to carry out this type of study since the snow accumulation is so limited that it is challenging to decipher whether any loss can be attributed to re-emission or wind erosion processes, exposing older layers, which generally have different bromine concentrations. In other parts of Antarctica, McConnell et al. (2017) suggest a bromine snow–air flux of loss of 17 ± 2 µg m^{-2} yr^{-1} re-

Table A1. Compilation Na/Mg, Na/Ca and Ca/Mg mass ratios in dust samples originating from north Asia deserts.

Ta et al. (2003)	Results of the X-ray fluorescence analysis of soil samples from the desert/Gobi areas in Gansu province, China								
	Desert areas							Gobi areas	
–	Dunhuang	Yumen	Anxi	Zhangye	Linze	Wuwei	Gulang	Yumen	Anxi
Na_2O (% ox)	1.97	2.05	1.19	1.46	1.76	1.59	1.47	1.36	2.62
MgO (% ox)	1.96	2	3	1.42	1.38	1.05	0.91	1.16	1.3
CaO (% ox)	6.5	6.31	10.59	2.21	2.95	2.23	2.23	8.4	4.88
Na (ppm)	14615	15208	8828	10831	13057	11796	10905	10089	19437
Mg (ppm)	11821	12062	18093	8564	8323	6333	5488	6996	7840
Ca (ppm)	46456	45098	75687	15795	21084	15938	15938	60035	34877
Na/Mg	1.24	1.26	0.49	1.26	1.57	1.86	1.99	1.44	2.48
Na/Ca	0.31	0.34	0.12	0.69	0.62	0.74	0.68	0.17	0.56
Ca/Mg	3.93	3.74	4.18	1.84	2.53	2.52	2.90	8.58	4.45

Wang et al. (2018)	Results of total suspended particle elemental concentrations in samples collected at Fudan University (Shanghai, China) during the 19 to 22 March 2010 dust storm estimated to originate from the Gobi Desert.				
–	19 Night	20 Day	20 Night	21 Day	21 Night
Na ($\mu g\,m^{-3}$)	1.3	7.9	19.1	2.8	3.9
Mg ($\mu g\,m^{-3}$)	1.4	9.5	14.4	2.2	2.3
Ca ($\mu g\,m^{-3}$)	8.5	37.3	56.9	9.4	8.6
Na/Mg	0.93	0.83	1.33	1.27	1.70
Na/Ca	0.15	0.21	0.34	0.30	0.45
Ca/Mg	6.07	3.93	3.95	4.27	3.74

Sun et al. (2005)	Elemental concentrations in aerosols sampled during two springtime 2002 desert storms that hit Beijing, both of which originated from north Asia deserts.	
–	Desert storm 1	Desert storm 2
Na ($\mu g\,m^{-3}$)	37	39
Mg ($\mu g\,m^{-3}$)	34	29
Ca ($\mu g\,m^{-3}$)	178	58
Na/Mg	1.09	1.34
Na/Ca	0.21	0.67
Ca/Mg	5.24	2.00

Fan et al. (2013)	Elemental concentrations measured in Guangzhou (China) during the 23–25 April 2009 dust storm originating in North China.
–	Desert storm
Na ($\mu g\,m^{-3}$)	2.98
Mg ($\mu g\,m^{-3}$)	2.83
Ca ($\mu g\,m^{-3}$)	5.78
Na/Mg	1.05
Na/Ca	0.52
Ca/Mg	2.04

Zhang et al. (2002)	Composition of air-volume-based concentration of aerosols sampled in Minquin (northwest China desert region) in March–May 1995 and April–June 1996.			
–	Minquin 1995		Minquin 1996	
–	Geometric mean	Average	Geometric mean	Average
Na ($\mu g\,m^{-3}$)	1.37	3.22	1.24	1.8
Mg ($\mu g\,m^{-3}$)	2.14	4.4	2.07	2.88
Ca ($\mu g\,m^{-3}$)	5.7	11.4	6.21	8.41
Na/Mg	0.64	0.73	0.60	0.63
Na/Ca	0.24	0.28	0.20	0.21
Ca/Mg	2.66	2.59	3.00	2.92

Wang et al. (2009)	Arithmetic mean elemental concentrations measured in $n = 317$ dust fallout samples collected from 33 sites located in the Gobi Desert, sandy desert, loess, and steppes in North China from April 2001 to March 2002.
Na (%)	1.47
Mg (%)	1.01
Ca (%)	3.40
Na/Mg	1.46
Na/Ca	0.43
Ca/Mg	3.37

gardless of snow accumulation, while at GV7 bromine loss was not detected (Vallelonga et al., QSR, 2019). In the Arctic, photolytic loss was not detected in Svalbard. Other experiments have been shown to be inconclusive due to the presence of surface melting. At sites like Renland (where Holocene melting occurs; see Taranczewski et al., 2019), the extremely high snow accumulation could in general suggest a reduced bromine loss, but again, the 5-fold decrease in snow accumulation during the glacial (preliminary $A_{\mathrm{glacial,stadials}} = 100\,\mathrm{kg\,m^{-2}\,yr^{-1}}$ (Bo M. Vinther, unpublished data)) may introduce a possible bromine loss during periods of reduced accumulation, thus increasing $\mathrm{Br_{enr}}$ values during the coldest parts of the record. To test these hypotheses and especially the bromine loss during the glacial, a surface study should be carried out at a $100\,\mathrm{kg\,m^{-2}\,yr^{-1}}$ accumulation site in Greenland. To conclude, at present there are not enough data available to quantify the possible bromine loss from the Renland ice cap, but if present, and depending on accumulation, the effect would be to increase the measured $\mathrm{Br_{enr}}$ values during the coldest sections of the glacial period.

Appendix B: Modern Na/Mg and Na/Ca ratios in dust from northern Asian deserts

The aim of this section is to obtain a reference value for the present-day mass ratios of Na/Mg and Na/Ca in Asian dust, since the Gobi and desert regions of Mongolian and northern China (hereafter referred to as Asian dust) are believed to be the main source regions of dust found in Greenlandic ice cores during the glacial period, as inferred from Sr, Nd and Pb isotope composition (Biscaye et al., 1997).

We consider $n = 6$ published studies in which the chemical composition of dust sampled during "desert events" (DSs) was analysed in China. Often these studies are carried out in the framework of pollution-related research. We also include composition data from dust sampled in situ in desert areas. For details on the single studies, we refer the reader to the references in Table A1. We note that our compilation only considers dust samples originating (or sampled directly) from deserts. Other geochemical data from such references that considered trajectories that travelled over other areas (marine or others), are not considered.

By considering all the above-mentioned studies, the mean Na/Mg mass ratio is 1.23 (median = 1.26). The mean Na/Ca mass ratio is 0.38 (median = 0.33). The mean Ca/Mg mass ratio is 3.66 (median = 3.55).

Appendix C: Bromine–sodium correlation in the RECAP ice core

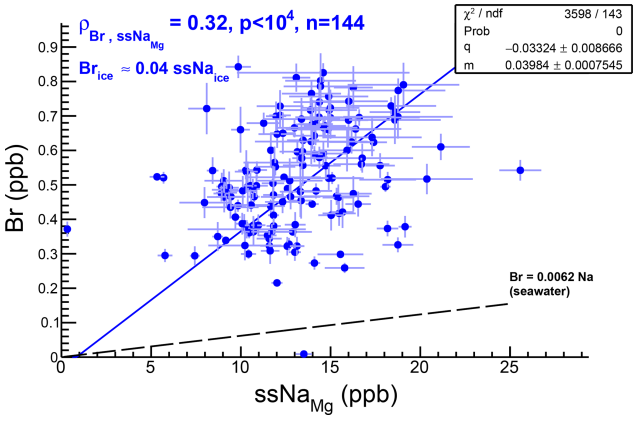

Figure C1. Correlation between bromine and $\mathrm{ssNa_{Mg}}$ concentrations in the glacial section of the RECAP ice core. The weak positive correlation suggests a common source for the two elements. The slope of the (qualitative, $p(\chi^2) \sim 0$) linear fit indicates significant (~ 6) enrichment compared to seawater mass ratios (black line).

Appendix D: Sensitivity of the $Br_{enr,Mg}$ and $Br_{enr,Cl}$ regimes to the NGRIP temperature threshold

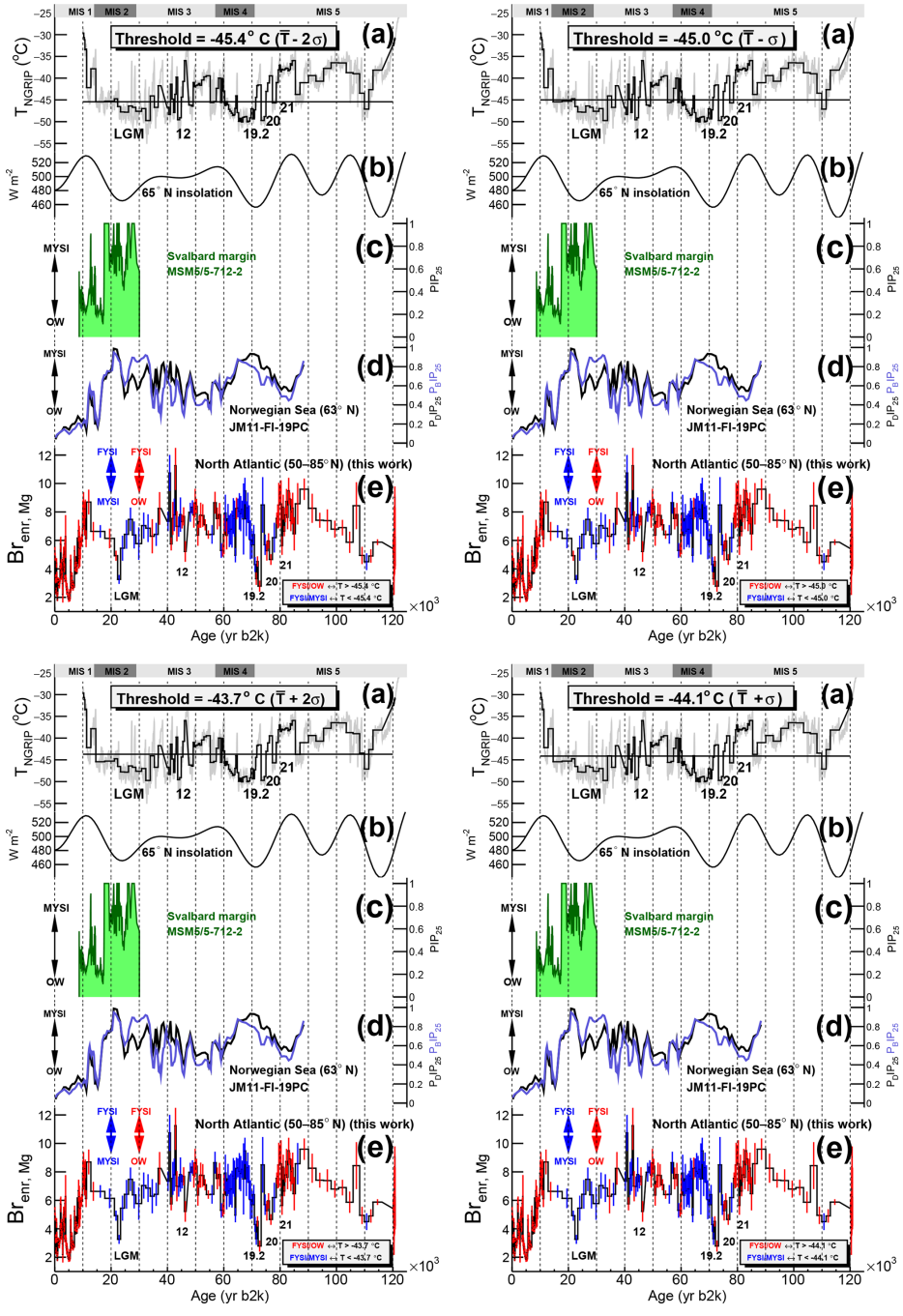

Figure D1. Sensitivity test of the NGRIP temperature threshold used to perform the $Br_{enr,Mg}$ regime discrimination (see Fig. D2 for the equivalent analysis using $Br_{enr,Cl}$). **(a)** Reconstructed NGRIP temperature (grey, Kindler et al., 2014). The temperature threshold value is the mean temperature ($\overline{T} \pm 2\sigma$: left; $T \pm 1\sigma$: right) during the 11.8–12.4 ka period, when the change in $Br_{enr,Mg}$ regime was observed (see Fig. 6). The black time series is the temperature profile downscaled to the measured Br_{enr} resolution. The numbers indicate the Greenland Interstadials (GIs) discussed in the text; **(b)** 21 June daily mean insolation at 65° N (Laskar et al., 2004); **(c)** PIP_{25} record from the Svalbard margin (core MSM5/5-712-2 from Müller and Stein, 2014); **(d)** 90 kyr P_DIP_{25} and P_BIP_{25} records from the Norwegian Sea presented as five-point running mean (from Hoff et al., 2016); **(e)** discrimination between the $Br_{enr,Mg}$ regimes computed according to the integrated temperature value with respect to the threshold. The FYSI/OW and FYSI/MYSI regimes are indicated with red and blue error bars respectively.

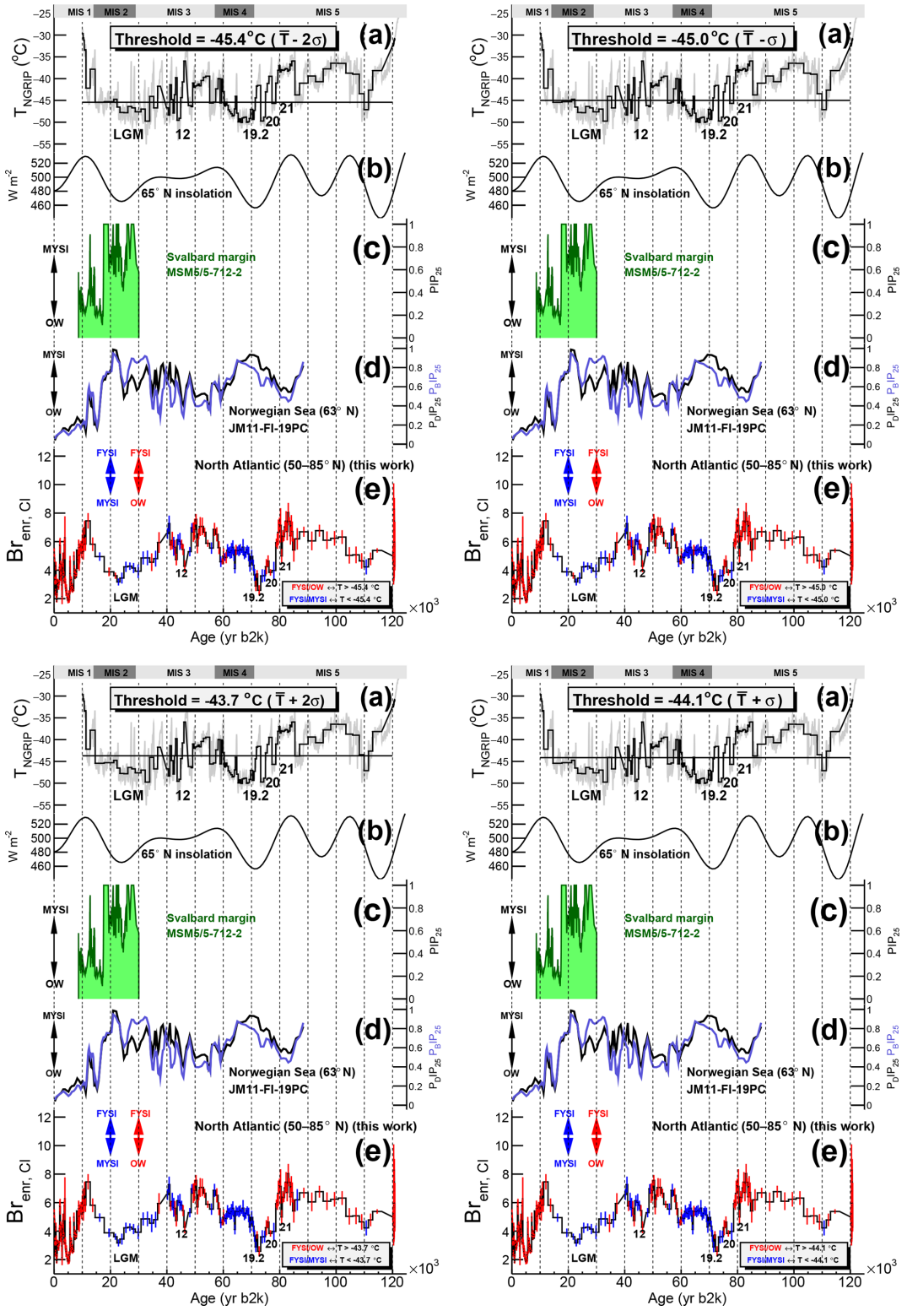

Figure D2. Discrimination between the two $Br_{enr,Cl}$ regimes according to the NGRIP temperature threshold. This figure is equivalent to Fig. D1 with $Br_{enr,Mg}$ replaced by $Br_{enr,Cl}$.

Author contributions. PV and AS conceived the experiment. NM, RE, PV, AS, HAK and CT collected the samples and ran the experimental analyses. NM analysed and interpreted the results. NM wrote the paper with inputs from all authors.

Competing interests. The authors declare that they have no conflict of interest.

Acknowledgements. We thank the whole Continuous Flow Analysis team at the Centre for Ice and Climate (Copenhagen, Denmark) for the sample collection. We thank Trevor Popp, Steffen Bo Hansen and the RECAP drilling group and Joel Pedro, Markus Jochum and Trond Dokken for the fruitful discussions. We thank the five reviewers for their constructive comments to improve the paper. We thank Zhao Meixun and Francesco Muschitiello for sharing the Icelandic and Norwegian core data. We thank Giovanni Baccolo for his useful insights.

Financial support. The RECAP ice coring effort was financed by the Danish Research Council through a Sapere Aude Grant, the NSF through the Division of Polar Programs, the Alfred Wegener Institute, and the European Research Council under the European Community's Seventh Framework Programme (FP7/2007-2013)/ERC grant agreement 610055 through the Ice2Ice project and the Early Human Impact project (grant agreement 267696). This study has also received funding from the European Research Council Executive Agency under the European Union's Horizon 2020 Research and Innovation programme (Project ERC-2016-COG 726349 CLIMAHAL).

Review statement. This paper was edited by Amaelle Landais and reviewed by five anonymous referees.

References

Abbatt, J.: Arctic snowpack bromine release, Nat. Geosci., 6, 331–332, https://doi.org/10.1038/ngeo1805, 2013.

Abbatt, J. P. D., Thomas, J. L., Abrahamsson, K., Boxe, C., Granfors, A., Jones, A. E., King, M. D., Saiz-Lopez, A., Shepson, P. B., Sodeau, J., Toohey, D. W., Toubin, C., von Glasow, R., Wren, S. N., and Yang, X.: Halogen activation via interactions with environmental ice and snow in the polar lower troposphere and other regions, Atmos. Chem. Phys., 12, 6237–6271, https://doi.org/10.5194/acp-12-6237-2012, 2012.

Ashbaugh, L. L., Malm, W. C., and Sadeh, W. Z.: A residence time probability analysis of sulfur concentrations at Grand Canyon National Park, Atmos. Environ., 19, 1263–1270, 1985.

Barrie, L., Bottenheim, J., Schnell, R., Crutzen, P., and Rasmussen, R.: Ozone destruction and photochemical reactions at polar sunrise in the lower Arctic atmosphere, Nature, 334, 138–141, 1988.

Belt, S. T. and Müller, J.: The Arctic sea ice biomarker IP 25: a review of current understanding, recommendations for future research and applications in palaeo sea ice reconstructions, Quaternary Sci. Rev., 79, 9–25, 2013.

Belt, S. T., Cabedo-Sanz, P., Smik, L., Navarro-Rodriguez, A., Berben, S. M., Knies, J., and Husum, K.: Identification of paleo Arctic winter sea ice limits and the marginal ice zone: optimised biomarker-based reconstructions of late Quaternary Arctic sea ice, Earth Planet. Sc. Lett., 431, 127–139, 2015.

Bereiter, B., Shackleton, S., Baggenstos, D., Kawamura, K., and Severinghaus, J.: Mean global ocean temperatures during the last glacial transition, Nature, 553, 39–44, https://doi.org/10.1038/nature25152, 2018.

Bigler, M., Svensson, A., Kettner, E., Vallelonga, P., Nielsen, M. E., and Steffensen, J. P.: Optimization of high-resolution continuous flow analysis for transient climate signals in ice cores, Environ. Sci. Technol., 45, 4483–4489, 2011.

Biscaye, P., Grousset, F., Revel, M., Van der Gaast, S., Zielinski, G., Vaars, A., and Kukla, G.: Asian provenance of glacial dust (stage 2) in the Greenland Ice Sheet Project 2 ice core, Summit, Greenland, J. Geophys. Res.-Oceans, 102, 26765–26781, 1997.

Buizert, C., Gkinis, V., Severinghaus, J. P., He, F., Lecavalier, B. S., Kindler, P., Leuenberger, M., Carlson, A. E., Vinther, B., Masson-Delmotte, V., White, J. W., Liu, Z., Otto-Bliesner, B., Brook, E. J.: Greenland temperature response to climate forcing during the last deglaciation, Science, 345, 1177–1180, https://doi.org/10.1126/science.1254961, 2014.

Cabedo-Sanz, P., Belt, S. T., Knies, J., and Husum, K.: Identification of contrasting seasonal sea ice conditions during the Younger Dryas, Quaternary Sci. Rev., 79, 74–86, 2013.

Cabedo-Sanz, P., Belt, S. T., Jennings, A. E., Andrews, J. T., and Geirsdóttir, Á.: Variability in drift ice export from the Arctic Ocean to the North Icelandic Shelf over the last 8000 years: a multi-proxy evaluation, Quaternary Sci. Rev., 146, 99–115, 2016.

Chance, K.: Analysis of BrO measurements from the global ozone monitoring experiment, Geophys. Res. Lett., 25, 3335–3338, 1998.

Corella, J. P., Maffezzoli, N., Cuevas, C. A., Vallelonga, P., Spolaor, A., Cozzi, G., Müller, J., Vinther, B., Barbante, C., Kjaer, H. A., Edwards, R., and Saiz-Lopez, A.: Holocene atmospheric iodine evolution over the North Atlantic, Clim. Past Discuss., https://doi.org/10.5194/cp-2019-71, in review, 2019.

Cuevas, C. A., Maffezzoli, N., Corella, J. P., Spolaor, A., Vallelonga, P., Kjær, H. A., Simonsen, M., Winstrup, M., Vinther, B., Horvat, C., Fernandez, R. P., Kinnison, D. E., Lamarque, J., Barbante, C., and Saiz-Lopez, A.: Rapid increase in atmospheric iodine levels in the North Atlantic since the mid-20th century, Nat. Commun., 9, 1452, https://doi.org/10.1038/s41467-018-03756-1, 2018.

De Angelis, M., Steffensen, J. P., Legrand, M., Clausen, H., and Hammer, C.: Primary aerosol (sea salt and soil dust) deposited in Greenland ice during the last climatic cycle: Comparison with east Antarctic records, J. Geophys. Res.-Oceans, 102, 26681–26698, 1997.

Dibb, J. E., Ziemba, L. D., Luxford, J., and Beckman, P.: Bromide and other ions in the snow, firn air, and atmospheric boundary layer at Summit during GSHOX, Atmos. Chem. Phys., 10, 9931–9942, https://doi.org/10.5194/acp-10-9931-2010, 2010.

Dokken, T. M. and Jansen, E.: Rapid changes in the mechanism of ocean convection during the last glacial period, Nature, 401, 458–461, 1999.

Draxler, R. and Hess, G.: Description of the HYSPLIT 4 modeling system NOAA Tech, NOAA Tech Memo ERL ARL-224, 24, 1997.

Draxler, R. R. and Hess, G.: An overview of the HYSPLIT_4 modelling system for trajectories, Aust. Meteorol. Mag., 47, 295–308, 1998.

Draxler, R. R., Stunder, B., Rolph, G., and Taylor, A.: HYSPLIT4 Users's Guide, US Department of Commerce, National Oceanic and Atmospheric Administration, Environmental Research Laboratories, Air Resources Laboratory, 1999.

Fan, Q., Shen, C., Wang, X., Li, Y., Huang, W., Liang, G., Wang, S., and Huang, Z.: Impact of a dust storm on characteristics of particle matter (PM) in Guangzhou, China, Asia-Pac. J. Atmos. Sci., 49, 121–131, 2013.

Frey, M. M., Norris, S. J., Brooks, I. M., Anderson, P. S., Nishimura, K., Yang, X., Jones, A. E., Nerentorp Mastromonaco, M. G., Jones, D. H., and Wolff, E. W.: First direct observation of sea salt aerosol production from blowing snow above sea ice, Atmos. Chem. Phys. Discuss., https://doi.org/10.5194/acp-2019-259, in review, 2019.

Hansson, M. E.: The Renland ice core. A Northern Hemisphere record of aerosol composition over 120,000 years, Tellus B, 46, 390–418, https://doi.org/10.1034/j.1600-0889.1994.t01-4-00005.x, 1994.

Hoff, U., Rasmussen, T. L., Stein, R., Ezat, M. M., and Fahl, K.: Sea ice and millennial-scale climate variability in the Nordic seas 90 [thinsp] kyr ago to present, Nat. Commun., 7, 12247, https://doi.org/10.1038/ncomms12247, 2016.

Kalnay, E., Kanamitsu, M., Kistler, R., Collins, W., Deaven, D., Gandin, L., Iredell, M., Saha, S., White, G., Woollen, J., Zhu, Y., Chelliah, M., Ebisuzaki, W., Higgins, W., Janowiak, J., Mo, K. C., Ropelewski, C., Wang, J., Leetmaa, A., Reynolds, R., Jenne, R., and Joseph, D.: The NCEP/NCAR 40-year reanalysis project, B. Am. Meteorol. Soc., 77, 437–471, 1996.

Kaufmann, P. R., Federer, U., Hutterli, M. A., Bigler, M., Schüpbach, S., Ruth, U., Schmitt, J., and Stocker, T. F.: An improved continuous flow analysis system for high-resolution field measurements on ice cores, Environ. Sci. Technol., 42, 8044–8050, 2008.

Kindler, P., Guillevic, M., Baumgartner, M., Schwander, J., Landais, A., and Leuenberger, M.: Temperature reconstruction from 10 to 120 kyr b2k from the NGRIP ice core, Clim. Past, 10, 887–902, https://doi.org/10.5194/cp-10-887-2014, 2014.

Kreher, K., Johnston, P., Wood, S., Nardi, B., and Platt, U.: Ground-based measurements of tropospheric and stratospheric BrO at Arrival Heights, Antarctica, Geophys. Res. Lett., 24, 3021–3024, 1997.

Laskar, J., Robutel, P., Joutel, F., Gastineau, M., Correia, A., and Levrard, B.: A long-term numerical solution for the insolation quantities of the Earth, Astron. Astrophys., 428, 261–285, 2004.

Legrand, M. and Mayewski, P.: Glaciochemistry of polar ice cores: a review, Rev. Geophys., 35, 219–243, 1997.

Legrand, M., Yang, X., Preunkert, S., and Theys, N.: Year-round records of sea salt, gaseous, and particulate inorganic bromine in the atmospheric boundary layer at coastal (Dumont d'Urville) and central (Concordia) East Antarctic sites, J. Geophys. Res.-Atmos., 121, 997–1023, 2016.

Legrand, M. R. and Delmas, R. J.: Formation of HCl in the Antarctic atmosphere, J. Geophys. Res.-Atmos., 93, 7153–7168, 1988.

Lewis, E. R. and Schwartz, S. E.: Sea salt aerosol production: mechanisms, methods, measurements, and models – A critical review, vol. 152, American Geophysical Union, 2004.

Li, C., Kang, S., Shi, G., Huang, J., Ding, M., Zhang, Q., Zhang, L., Guo, J., Xiao, C., Hou, S., Sun, B., Qin, D., and Ren, R.: Spatial and temporal variations of total mercury in Antarctic snow along the transect from Zhongshan Station to Dome A, Tellus B, 66, 25152, https://doi.org/10.3402/tellusb.v66.25152, 2014.

Maffezzoli, N., Spolaor, A., Barbante, C., Bertò, M., Frezzotti, M., and Vallelonga, P.: Bromine, iodine and sodium in surface snow along the 2013 Talos Dome–GV7 traverse (northern Victoria Land, East Antarctica), The Cryosphere, 11, 693–705, https://doi.org/10.5194/tc-11-693-2017, 2017.

Maggi, V.: Mineralogy of atmospheric microparticles deposited along the Greenland Ice Core Project ice core, J. Geophys. Res.-Oceans, 102, 26725–26734, 1997.

Mayewski, P. A., Meeker, L. D., Whitlow, S., Twickler, M. S., Morrison, M. C., Bloomfield, P., Bond, G., Alley, R. B., Gow, A. J., Meese, D. A., Ram M., Taylor, K. C., and Wumkes, W.: Changes in atmospheric circulation and ocean ice cover over the North Atlantic during the last 41 000 years, Science, 263, 1747–1751, 1994.

McConnell, J. R., Maselli, O. J., Sigl, M., Vallelonga, P., Neumann, T., Anschütz, H., Bales, R. C., Curran, M. A., Das, S. B., Edwards, R., Kipfstuhl, S., Layman, L., and Thomas, E. R.: Antarctic-wide array of high-resolution ice core records reveals pervasive lead pollution began in 1889 and persists today, Sci. Rep., 4, 5848, https://doi.org/0.1038/srep05848, 2014.

McConnell, J. R., Burke, A., Dunbar, N. W., Köhler, P., Thomas, J. L., Arienzo, M. M., Chellman, N. J., Maselli, O. J., Sigl, M., Adkins, J. F., Baggenstos, D., Burkhart, J. F. , Brook, E. J., Buizert, C., Cole-Dai, J., Fudge, T. J., Knorr, G., Graf, H.-F., Grieman, M. M., Iverson, N., McGwire, K. C., Mulvaney, R., Paris, G., Rhodes, R. H., Saltzman, E. S., Severinghaus, J. P., Steffensen, J. P., Taylor, K. C., and Winckler, G.: Synchronous volcanic eruptions and abrupt climate change 17.7 ka plausibly linked by stratospheric ozone depletion, P. Natl. Acad. Sci. USA, 114, 10035–10040, 2017.

McManus, J. F., Francois, R., Gherardi, J.-M., Keigwin, L. D., and Brown-Leger, S.: Collapse and rapid resumption of Atlantic meridional circulation linked to deglacial climate changes, Nature, 428, 834–837, https://doi.org/10.1038/nature02494, 2004.

Millero, F. J., Feistel, R., Wright, D. G., and McDougall, T. J.: The composition of Standard Seawater and the definition of the Reference-Composition Salinity Scale, Deep Sea-Res. Pt. I, 55, 50–72, https://doi.org/10.1016/j.dsr.2007.10.001, 2008.

Müller, J. and Stein, R.: High-resolution record of late glacial and deglacial sea ice changes in Fram Strait corroborates ice–ocean interactions during abrupt climate shifts, Earth Planet. Sc. Lett., 403, 446–455, 2014.

Müller, J., Wagner, A., Fahl, K., Stein, R., Prange, M., and Lohmann, G.: Towards quantitative sea ice reconstructions in the northern North Atlantic: a combined biomarker and numerical modelling approach, Earth Planet. Sc. Lett., 306, 137–148, 2011.

Muschitiello, F., D'Andrea, W. J., Schmittner, A., Heaton, T. J., Balascio, N. L., DeRoberts, N., Caffee, M. W., Woodruff, T. E., Welten, K. C., Skinner, L. C., Simon, M. H., and Dokken, T. M.: Deep-water circulation changes lead North At-

lantic climate during deglaciation, Nat. Commun., 10, 1272, https://doi.org/10.1038/s41467-019-09237-3, 2019.

North Greenland Ice Core Project members: High-resolution record of Northern Hemisphere climate extending into the last interglacial period, Nature, 431, 147–151, 2004.

Pratt, K. A., Custard, K. D., Shepson, P. B., Douglas, T. A., Pöhler, D., General, S., Zielcke, J., Simpson, W. R., Platt, U., Tanner, D. J., Huey, L. G., Carlsen, M., and Stirm, B. H.: Photochemical production of molecular bromine in Arctic surface snowpacks, Nat. Geosci., 6, 351–356, 2013.

Rhodes, R. H., Yang, X., and Wolff, E. W.: Sea Ice Versus Storms: What Controls Sea Salt in Arctic Ice Cores?, Geophys. Res. Lett., 45, 5572–5580, https://doi.org/10.1029/2018GL077403, 2018.

Richter, A., Wittrock, F., Eisinger, M., and Burrows, J. P.: GOME observations of tropospheric BrO in northern hemispheric spring and summer 1997, Geophys. Res. Lett., 25, 2683–2686, 1998.

Ritz, S. P., Stocker, T. F., Grimalt, J. O., Menviel, L., and Timmermann, A.: Estimated strength of the Atlantic overturning circulation during the last deglaciation, Nat. Geosci., 6, 208–212, https://doi.org/10.1038/ngeo1723, 2013.

Röthlisberger, R., Mulvaney, R., Wolff, E. W., Hutterli, M. A., Bigler, M., Sommer, S., and Jouzel, J.: Dust and sea salt variability in central East Antarctica (Dome C) over the last 45 kyrs and its implications for southern high-latitude climate, Geophys. Res. Lett., 29, 1963, https://doi.org/10.1029/2002GL015186, 2002.

Röthlisberger, R., Mulvaney, R., Wolff, E. W., Hutterli, M. A., Bigler, M., De Angelis, M., Hansson, M. E., Steffensen, J. P., and Udisti, R.: Limited dechlorination of sea-salt aerosols during the last glacial period: Evidence from the European Project for Ice Coring in Antarctica (EPICA) Dome C ice core, J. Geophys. Res.-Atmos., 108, 4526, https://doi.org/10.1029/2003JD003604, 2003.

Rudnick, R. and Gao, S.: Composition of the continental crust, Treatise on Geochemistry, 3, 659 pp., 2003.

Saiz-Lopez, A. and von Glasow, R.: Reactive halogen chemistry in the troposphere, Chem. Soc. Rev., 41, 6448–6472, 2012.

Schüpbach, S., Fischer, H., Bigler, M., Erhardt, T., Gfeller, G., Leuenberger, D., Mini, O., Mulvaney, R., Abram, N. J., Fleet, L., Frey, M. M., Thomas, E., Svensson, A., Dahl-Jensen, D., Kettner, E., Kjaer, H., Seierstad, I., Steffensen, J. P., Rasmussen, S. O., Vallelonga, P., Winstrup, M., Wegner, A., Twarloh, B., Wolff, K., Schmidt, K., Goto-Azuma, K., Kuramoto, T., Hirabayashi, M., Uetake, J., Zheng, J., Bourgeois, J., Fisher, D., Zhiheng, D., Xiao, C., Legrand, M., Spolaor, A., Gabrieli, J., Barbante, C., Kang, J. H., Hur, S. D., Hong, S. B., Hwang, H. J., Hong, S., Hansson, M., Iizuka, Y., Oyabu, I., Muscheler, R., Adolphi, F., Maselli, O., McConnell, J., and Wolff, E. W.: Greenland records of aerosol source and atmospheric lifetime changes from the Eemian to the Holocene, Nat. Commun., 9, 1476, https://doi.org/10.1038/s41467-018-03924-3, 2018.

Simonsen, M. F., Baccolo, G., Blunier, T., Borunda, A., Delmonte, B., Frei, R., Goldstein, S., Grinsted, A., Kjær, H. A., Sowers, T., Svensson, A., Vinther, B., Vladimirova, D., Winckler, G., Winstrup, M., and Vallelonga, P.: East Greenland ice core dust record reveals timing of Greenland ice sheet advance and retreat, Nat. Commun., 10, 1–8, 2019.

Simpson, W. R., Alvarez-Aviles, L., Douglas, T. A., Sturm, M., and Domine, F.: Halogens in the coastal snow pack near Barrow, Alaska: Evidence for active bromine air-snow chemistry during springtime, Geophys. Res. Lett., 32, L04811, https://doi.org/10.1029/2004GL021748, 2005.

Spolaor, A., Gabrieli, J., Martma, T., Kohler, J., Björkman, M. B., Isaksson, E., Varin, C., Vallelonga, P., Plane, J. M. C., and Barbante, C.: Sea ice dynamics influence halogen deposition to Svalbard, The Cryosphere, 7, 1645–1658, https://doi.org/10.5194/tc-7-1645-2013, 2013a.

Spolaor, A., Vallelonga, P., Plane, J. M. C., Kehrwald, N., Gabrieli, J., Varin, C., Turetta, C., Cozzi, G., Kumar, R., Boutron, C., and Barbante, C.: Halogen species record Antarctic sea ice extent over glacial–interglacial periods, Atmos. Chem. Phys., 13, 6623–6635, https://doi.org/10.5194/acp-13-6623-2013, 2013b.

Spolaor, A., Vallelonga, P., Gabrieli, J., Martma, T., Björkman, M. P., Isaksson, E., Cozzi, G., Turetta, C., Kjær, H. A., Curran, M. A. J., Moy, A. D., Schönhardt, A., Blechschmidt, A.-M., Burrows, J. P., Plane, J. M. C., and Barbante, C.: Seasonality of halogen deposition in polar snow and ice, Atmos. Chem. Phys., 14, 9613–9622, https://doi.org/10.5194/acp-14-9613-2014, 2014.

Spolaor, A., Opel, T., McConnell, J. R., Maselli, O. J., Spreen, G., Varin, C., Kirchgeorg, T., Fritzsche, D., Saiz-Lopez, A., and Vallelonga, P.: Halogen-based reconstruction of Russian Arctic sea ice area from the Akademii Nauk ice core (Severnaya Zemlya), The Cryosphere, 10, 245–256, https://doi.org/10.5194/tc-10-245-2016, 2016a.

Spolaor, A., Vallelonga, P., Turetta, C., Maffezzoli, N., Cozzi, G., Gabrieli, J., Barbante, C., Goto-Azuma, K., Saiz-Lopez, A., Cuevas, C. A., and Dahl-Jensen, D.: Canadian Arctic sea ice reconstructed from bromine in the Greenland NEEM ice core, Sci. Rep., 6, 33925, https://doi.org/10.1038/srep33925, 2016b.

Spolaor, A., Angot, H., Roman, M., Dommergue, A., Scarchilli, C., Vardè, M., Del Guasta, M., Pedeli, X., Varin, C., Sprovieri, F., Magand, O., Legrand, M., Barbante, C., and Cairns, W. R. L.: Feedback mechanisms between snow and atmospheric mercury: Results and observations from field campaigns on the Antarctic plateau, Chemosphere, 197, 306–317, 2018.

Spolaor, A., Barbaro, E., Cappelletti, D., Turetta, C., Mazzola, M., Giardi, F., Björkman, M. P., Lucchetta, F., Dallo, F., Pfaffhuber, K. A., Angot, H., Dommergue, A., Maturilli, M., Saiz-Lopez, A., Barbante, C., and Cairns, W. R. L.: Diurnal cycle of iodine, bromine, and mercury concentrations in Svalbard surface snow, Atmos. Chem. Phys., 19, 13325–13339, https://doi.org/10.5194/acp-19-13325-2019, 2019.

Stein, A., Draxler, R. R., Rolph, G. D., Stunder, B. J., Cohen, M., and Ngan, F.: NOAA's HYSPLIT atmospheric transport and dispersion modeling system, B. Am. Meteorol. Soc., 96, 2059–2077, 2015.

Sun, Y., Zhuang, G., Wang, Y., Zhao, X., Li, J., Wang, Z., and An, Z.: Chemical composition of dust storms in Beijing and implications for the mixing of mineral aerosol with pollution aerosol on the pathway, J. Geophys. Res.-Atmos., 110, D24209, https://doi.org/10.1029/2005JD006054, 2005.

Ta, W., Xiao, Z., Qu, J., Yang, G., and Wang, T.: Characteristics of dust particles from the desert/Gobi area of northwestern China during dust-storm periods, Environ. Geol., 43, 667–679, 2003.

Taranczewski, T., Freitag, J., Eisen, O., Vinther, B., Wahl, S., and Kipfstuhl, S.: 10,000 years of melt history of the 2015 Renland ice core, EastGreenland, The Cryosphere Discuss., https://doi.org/10.5194/tc-2018-280, 2019.

Tschudi, M., Fowler, C., Maslanik, J., Stewart, J. S., and Meier, W. N.: EASE-Grid Sea Ice Age, Version 3. Boulder, Colorado USA, in: NASA National Snow and Ice Data Center Distributed Active Archive Center, https://doi.org/10.5067/PFSVFZA9Y85G, 2016.

Vallelonga, P., Maffezzoli, N., Moy, A. D., Curran, M. A. J., Vance, T. R., Edwards, R., Hughes, G., Barker, E., Spreen, G., Saiz-Lopez, A., Corella, J. P., Cuevas, C. A., and Spolaor, A.: Sea-ice-related halogen enrichment at Law Dome, coastal East Antarctica, Clim. Past, 13, 171–184, https://doi.org/10.5194/cp-13-171-2017, 2017.

Vogt, R., Crutzen, P. J., and Sander, R.: A mechanism for halogen release from sea-salt aerosol in the remote marine boundary layer, Nature, 383, 327–330, 1996.

Wagner, T. and Platt, U.: Satellite mapping of enhanced BrO concentrations in the troposphere, Nature, 395, 486–490, https://doi.org/10.1038/26723, 1998.

Wang, Q., Dong, X., Fu, J. S., Xu, J., Deng, C., Jiang, Y., Fu, Q., Lin, Y., Huang, K., and Zhuang, G.: Environmentally dependent dust chemistry of a super Asian dust storm in March 2010: observation and simulation, Atmos. Chem. Phys., 18, 3505–3521, https://doi.org/10.5194/acp-18-3505-2018, 2018.

Wang, X., Dong, Z., Zhang, C., Qian, G., and Luo, W.: Characterization of the composition of dust fallout and identification of dust sources in arid and semiarid North China, Geomorphology, 112, 144–157, 2009.

Wolff, E. W., Moore, J. C., Clausen, H. B., Hammer, C. U., Kipfstuhl, J., and Fuhrer, K.: Long-term changes in the acid and salt concentrations of the Greenland Ice Core Project ice core from electrical stratigraphy, J. Geophys. Res.-Atmos., 100, 16249–16263, 1995.

Xiao, X., Zhao, M., Knudsen, K. L., Sha, L., Eiríksson, J., Gudmundsdóttir, E., Jiang, H., and Guo, Z.: Deglacial and Holocene sea–ice variability north of Iceland and response to ocean circulation changes, Earth Planet. Sc. Lett., 472, 14–24, 2017.

Yang, X., Pyle, J. A., and Cox, R. A.: Sea salt aerosol production and bromine release: Role of snow on sea ice, Geophys. Res. Lett., 35, 16815, https://doi.org/10.1029/2008GL034536, 2008.

Yang, X., Pyle, J. A., Cox, R. A., Theys, N., and Van Roozendael, M.: Snow-sourced bromine and its implications for polar tropospheric ozone, Atmos. Chem. Phys., 10, 7763–7773, https://doi.org/10.5194/acp-10-7763-2010, 2010.

Zhang, J., Wu, Y., Liu, C., Shen, Z., and Zhang, Y.: Major components of aerosols in North China: Desert region and the Yellow Sea in the spring and summer of 1995 and 1996, J. Atmos. Sci., 59, 1515–1532, 2002.

Zhao, X., Strong, K., Adams, C., Schofield, R., Yang, X., Richter, A., Friess, U., Blechschmidt, A.-M., and Koo, J.-H.: A case study of a transported bromine explosion event in the Canadian high arctic, J. Geophys. Res.-Atmos., 121, 457–477, 2016.